nature communications

Article | Article in Press

https://doi.org/10.1038/s41467-026-78229-x

Transient efferocytosis-induced activation of IKKβ reprograms macrophages to promote tissue resolution in mice

Received: 1 January 2026

Accepted: 9 September 2026

Published online: 26 October 2026

Check for updates

David Ngai[1,10], Saheli Chowdhury[1,10], Santosh R. Sukka[1], George Kuriakose[1], Brian Havens[1], Mustafa Yalcinkaya[1], Jeremy M. Frey[2,3], Heather Doviak[4], Jennifer W. Bradford[5], Bernhard Dorweiler[6], Hanna Winter[7], Lars Maegdefessel[7], Kenneth Walsh[4], Joshua P. Thaler[2,3], Alan R. Tall[1] & Ira Tabas[1,8,9]

The clearance of apoptotic cells by macrophages, termed efferocytosis, activates multiple pro-resolving pathways, but whether there is a common upstream regulator remains unknown. Here, we report that in efferocytosing macrophages, MerTK activation by apoptotic cells rapidly and transiently activates IKKβ-NFκB and p38, which then promotes interleukin-10 (IL-10) production, continuing efferocytosis, and regulatory T cell expansion. The IKKβ/p38 and downstream resolution pathways are linked through the transcription factor Myc, the epigenetic modifier ten-eleven translocation-2 (TET2), and the immune checkpoint protein programmed cell death ligand 1 (PD-L1). Deletion of macrophage IKKβ in male mice blocks the above resolution pathways and compromises efferocytosis-mediated tissue repair in a model of thymic injury and in atherosclerosis regression. Thus, our findings illustrate the existence of a unifying upstream signal for efferocytosis-induced resolution, which could suggest therapeutic strategies to enhance multiple tissue resolution pathways and to optimize anti-inflammatory therapies by avoiding blocking IKKβ-NFκB/p38-mediated resolution.

The clearance of apoptotic cells (AC) by macrophages, termed efferocytosis, is a critical process that both prevents secondary necrosis and subsequent inflammation and promotes tissue repair and inflammation resolution[1–4]. Efferocytosis-induced resolution involves the reprogramming of macrophages to produce molecules that promote tissue repair, e.g., interleukin-10 (IL-10) and transforming growth factor-β1 (TGF-β1); induce Myc-mediated proliferation of pro-resolving macrophages; and enable macrophages to sequentially clear multiple ACs by a key specialized process called continuing efferocytosis, leading to a positive-feedback cycle[5–9]. The efferocytosis-resolution cycle is critical for maintaining tissue homeostasis, and its pathological disruption drives many chronic inflammatory diseases[1–4]. Accordingly, understanding how efferocytosis reprograms macrophages to become pro-resolving represents a fundamental and therapeutically relevant goal of research investigating the roles of innate immunity in tissue homeostasis, resolution, and disease. Previous work has identified

[1]Department of Medicine, Columbia University Irving Medical Center, New York, NY, USA. [2]UW Medicine Diabetes Institute, University of Washington, Seattle, WA, USA. [3]Department of Medicine, University of Washington, Seattle, WA, USA. [4]Hematovascular Biology Center, Robert M. Berne Cardiovascular Research Center, University of Virginia School of Medicine, Charlottesville, VA, USA. [5]Department of Biological Sciences, Augusta University, Augusta, GA, USA. [6]Department of Vascular and Endovascular Surgery, University of Cologne, Faculty of Medicine and University Hospital Cologne, Cologne, Germany. [7]Institute of Molecular Vascular Medicine, TUM KlinikumTechnical University of Munich, Munich, Germany. [8]Department of Physiology and Cellular Biophysics, Columbia University Irving Medical Center, New York, NY, USA. [9]Department of Pathology, Columbia University Irving Medical Center, New York, NY, USA. [10]These authors contributed equally: David Ngai, Saheli Chowdhury. e-mail: iat1@columbia.edu

multiple downstream pathways that link efferocytosis to resolution signaling, some of which involve the metabolism of molecules derived from the phagolysosomal degradation of ACs, e.g., amino acids and nucleotides[8–15]. A major gap that remains, however, is determining whether there is a common upstream signal that orchestrates many of the distinct downstream pro-resolving pathways that have been identified thus far.

In this study, we investigate very early events in efferocytosis to identify a common upstream initiating signal for multiple downstream resolution pathways. We report that AC-induced activation of the efferocytosis receptor MerTK transiently increases the phosphorylation (activation) of inhibitor of nuclear factor kappa-B kinase (NFκB) subunit beta (IKKβ), leading to activation of both NFκB and p38. This upstream event is required for the efferocytosis-induced upregulation of multiple pro-resolving processes, including IL-10 production, continuing efferocytosis, and induction of PD-L1. Most importantly, macrophage-specific deletion of IKKβ in two in vivo models, including atherosclerosis regression, leads to impairments of resolution signaling and continuing efferocytosis and increased tissue necrosis. These findings uncover a common upstream pathway in macrophages that links efferocytosis to multiple downstream resolution pathways. The involvement of signaling molecules that are typically used for pro-inflammatory signaling in macrophages in this upstream pathway has interesting cell biological and therapeutic implications.

Results

Efferocytosis transiently activates NFκB and p38 through IKK

During our investigation of signaling pathways that occur early in efferocytosis, we made the unexpected discovery that exposure of mouse bone marrow-derived macrophages (BMDM) to apoptotic Jurkat cells (ACs) for 45 min led to the phosphorylation of both the p65 subunit of NFκB and p38, indicating their activation (Fig. 1a). We also observed these increases in human monocyte-derived macrophages (HMDM) incubated with ACs (Fig. 1b) and in BMDMs incubated with apoptotic macrophages (Fig. 1c). We also determined if the activation of NFκB was through the canonical pathway, which involves the phosphorylation-induced ubiquitination and subsequent proteasomal degradation of IκBα (nuclear factor of kappa light polypeptide gene enhancer in B-cells inhibitor, alpha), leading to the activation of NFκB and its translocation to the nucleus[16]. As expected, there was a decrease in IκBα protein after 30 min of AC incubation (Fig. 1d).

The activation of NFκB and p38 was transient, with p-p65 and p-p38 increasing at 15 min after AC incubation and diminishing substantially in macrophages incubated with ACs for 45 min and then chased in the absence of ACs for 1–24 h (Fig. 1e). To rule out endotoxin contamination as the cause of NFκB activation, we treated efferocytosing macrophages with the endotoxin-inactivating reagent polymyxin B (PMB). AC-induced NFκB activation was not affected by PMB (Supplementary Fig. 1a), whereas LPS-induced NFκB activation was blocked by PMB (Supplementary Fig. 1b). We then definitively proved that the transient efferocytosis-induced activation of NFκB and p38 was not due to endotoxin contamination by showing their activation in efferocytosing macrophages in vivo. For this purpose, we used the well-validated dexamethasone-thymus model, in which thymocyte apoptosis is induced 4 h after i.p. injection of mice with dexamethasone (DEX), followed by efferocytosis of the apoptotic thymocytes by monocyte-derived thymic macrophages[10,17]. Accordingly, the thymi of mice were analyzed 4 and 8 h after injection with DEX or PBS control. We used immunostaining to identify phospho-p65 and phospho-p38 in efferocytosing thymic macrophages, defined as $Mac2^+$ cells with cytoplasmic TUNEL ($cTUN^+$), versus non-efferocytosing macrophages, defined as $Mac2^+$ $cTUN^-$ cells[17]. The data show that both phospho-p65 and phospho-p38 were higher in $cTUN^+$ versus $cTUN^-$ macrophages in the thymi of dexamethasone-treated mice at the 4-h timepoint, and this increase was significantly diminished by 8 h after injection (Fig. 1f and Supplementary Fig. 1c), consistent with the transient nature of the response seen in vitro.

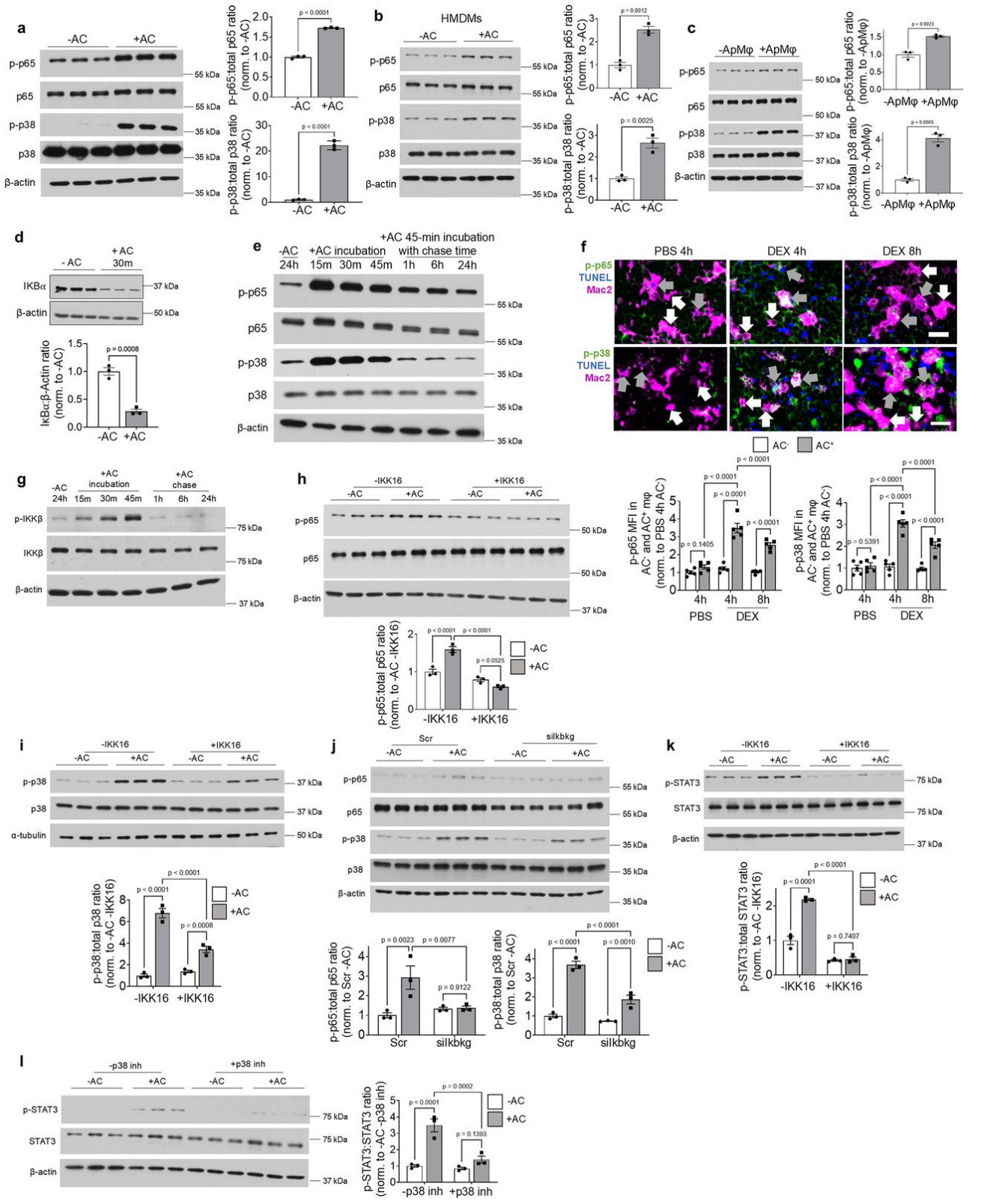
Activation of IKKβ leads to the phosphorylation/activation of p65 to trigger NFκB activation in inflammatory settings[18]. To determine the role of IKKβ in efferocytosis-induced activation of NFκB, we assayed IKKβ phosphorylation as a measure of its activation[18]. Incubation of macrophages with ACs led to the rapid and transient phosphorylation of IKKβ (Fig. 1g), as did incubation of macrophages with apoptotic macrophages (Supplementary Fig. 1d). Moreover, inhibition of IKKβ activity using the inhibitor IKK16[19] blocked efferocytosis-induced phospho-p65 (Fig. 1h). This effect was due to neither IKK16 decreasing primary efferocytosis (Supplementary Fig. 1e) nor to changes in phagolysosomal acidification, which was assayed by using ACs labeled with the acid-sensitive dye, pHrodo (Supplementary Fig. 1f). We next turned our attention to p38. While the efferocytosis-induced increase in phospho-p38 was not significantly blocked in p65-knockout BMDMs (Supplementary Fig. 1g), phospho-p38 was blocked by inhibiting IKKβ with IKK16 (Fig. 1i), suggesting a link between IKKβ and p38 phosphorylation. As further evidence for this link, partial silencing of another key component of the IKK complex, IKKγ/NFκB essential modulator (NEMO)[20], not only blocked phospho-p65 as expected but also partially lowered the level of phospho-p38 (Fig. 1j and Supplementary Fig. 1h). Finally, we investigated a possible link between p38 and STAT3 in efferocytosing macrophages based on a previous study exploring the uptake of cancer cells by a tumor-derived myeloid cell line[21]. We found that exposure of macrophages to apoptotic Jurkat cells caused an increase in phospho-STAT3, which was blocked by both IKK16 and the p38 inhibitor SB203580[22] (Fig. 1k, l). As was the case with IKK16 (above), the p38 inhibitor did not affect primary efferocytosis (Supplementary Fig. 1i). IKKβ-induced phosphorylation of p65 was independent of IKKβ-induced activation of phospho-p38, as p38 inhibition did not affect AC-induced phospho-p65 (Supplementary Fig. 1j). In summary, exposure of macrophages to ACs activates IKKβ, which leads to the activation of both NFκB and p38-STAT3 via independent pathways.

MerTK activation by ACs triggers the IKKβ-NFκB-p38 pathway in macrophages

Efferocytosis begins with the binding of ACs to specialized cell-surface receptors on macrophages, followed by AC engulfment and degradation in phagolysosomes[16]. Previous work has shown that signaling reactions in macrophages can be triggered through the activation of efferocytosis receptors and/or by molecules released following the degradation of ACs in phagolysosomes, which can be blocked by the lysosomal acidification inhibitor bafilomycin[17]. Pre-treatment of macrophages with bafilomycin did not block AC-induced phospho-p65 (NFκB) or phospho-p38 (Supplementary Fig. 2a), suggesting that molecules released from the phagolysosomal degradation of ACs are not responsible for their activation. This finding is consistent with the rapid kinetics of activation. We therefore hypothesized that AC binding to an efferocytosis receptor triggers the activation of NFκB and p38. Given the critical role of MerTK signaling in efferocytosing macrophages[9,21,23,24], we tested the effect of silencing MerTK. We found that siMertk blocked AC-induced activation of p65, p38, and IKKβ (Fig. 2a, b). In contrast, silencing a MerTK-related receptor, Axl[25], did not block the efferocytosis-induced increase in p-IKKβ (Supplementary Fig. 2b). Similarly, silencing another efferocytosis receptor, LRP1, also did not block AC-induced p65 and p38 (Supplementary Fig. 2c). As further evidence for the involvement of MerTK, inhibition of MerTK kinase activity with UNC5293[26] blocked AC-induced p-IKKβ (Fig. 2c), and incubation of macrophages with the MerTK activator Gas6[27] led to a transient increase in p-IKKβ (Fig. 2d).

Given the upstream role of IKKβ and IKKγ in the pathway (above), we immunoprecipitated MerTK and then immunoblotted for phospho-IKKβ and total IKKγ in macrophages not exposed to ACs (basal) or

https://doi.org/10.1038/s41467-026-78229-x



exposed to ACs for 45 min (pulse) ± a 1 h chase. Compared to basal or 1 h chase macrophages, the AC-pulsed macrophages showed increased interaction of MerTK with phospho-IKKβ and IKKγ (Fig. 2e). Furthermore, the AC-mediated interaction between MerTK and IKKγ was dependent on MerTK kinase activity, as the MerTK kinase inhibitor UNC5293 prevented this interaction (Fig. 2f). Efferocytosis receptors are internalized after AC binding as part of the engulfment stage of efferocytosis[16]. We therefore considered the possibility that the transient nature of IKKβ activation might be due to internalization of the MerTK-IKK complex soon after AC binding. Internalization of phagosomes containing AC-bound efferocytosis receptors requires actin polymerization[16], which can be disrupted by cytochalasin D[10,11,17,28]. Accordingly, we compared the duration of AC-induced phospho-p65 in control versus cytochalasin-treated macrophages. Phospho-p65 was

Fig. 1 | Efferocytosis transiently activates NFκB and p38. a BMDMs) or **b** HMDMs) were incubated ± apoptotic Jurkat cells (ACs) for 45 min and immunoblotted for phospho- and total p65 and p38 ($n = 3$). **c** BMDMs were incubated ± apoptotic HMDMs (ApMφs) for 45 min and immunoblotted as in panel a ($n = 3$). **d** BMDMs were incubated ± ACs for 30 min and immunoblotted for IκBα ($n = 3$). **e** BMDMs were incubated with ACs for 15, 30, or 45 min, or incubated with ACs for 45 min and chased for 1, 6, or 24 h and immunoblotted as in panel a ($n = 3$). **f** Mice were injected with PBS or dexamethasone (DEX), and thymi were collected 4 or 8 h later. Thymic sections were labeled with TUNEL (blue) and immunostained for Mac2 (magenta) and phospho-p65 or phospho-p38 (green) and quantified for the MFI of phospho-p65 or phospho-p38 in cytoplasmic TUNEL$^+$ (AC$^+$) or cytoplasmic TUNEL$^-$ (AC$^-$) macrophages. Sections were imaged with a 20x objective. Scale bar, 20 μm ($n = 5$). White arrows, AC$^-$ macrophages; gray arrows, AC$^+$ macrophages. Overlap of Mac2 and phospho-p65 or phospho-p38 appears white in the images. **g** BMDMs incubated with ACs and chased for different periods were immunoblotted for phospho-IKKβ and total IKKβ ($n = 3$). **h**, **i** BMDMs pre-treated ± 500 nM IKK16 for 2 h were incubated ± ACs for 45 min and immunoblotted for phospho- and total p65 and p38 ($n = 3$). **j** BMDMs treated with scrambled RNA or siIkbkg were incubated ± ACs for 45 min and immunoblotted for phospho- and total p65 and p38 ($n = 3$). **k** BMDMs pre-treated ± 500 nM IKK16 for 2 h were incubated ± ACs for 45 min, chased for 1 h, and immunoblotted for p-STAT3 and total STAT3 ($n = 3$). **l** BMDMs pre-treated ± 10 μM SB203580 (p38 inh) for 2 h were incubated ± ACs for 45 min, chased for 1 h, and immunoblotted as in panel k ($n = 3$). Data are normalized to the first control group in each experiment. Bars represent means ± SEM. Statistics were performed using the Student's *t*-test in **a**–**d** and two-way ANOVA in (**f**, **h**–**l**).

elevated in both control and cytochalasin D-treated macrophages after a 45-min incubation with ACs (Fig. 2g). Consistent with the data above in Fig. 1e, the control macrophages showed much less phospho-p65 after a 1-h chase, whereas the cytochalasin D-treated cells showed no decrease in phospho-p65 at this time point (Fig. 2g). When considered together, these data are consistent with the idea that activation of MerTK kinase by ACs in the initial stage of efferocytosis orchestrates the transient activation of the IKK complex to activate p65 (NFκB) and p38. The transient nature of this pathway depends on a dynamic actin cytoskeleton, which, pending further investigation, may be due to deactivation of the MerTK-IKK complex upon its internalization into phagosomes.

Although MerTK kinase inhibition blocks the association of MerTK with IKKγ (above), MerTK is a tyrosine kinase, whereas IKKβ is mainly phosphorylated on serine residues for its activation[18]. We therefore explored the hypothesis that AC-mediated activation of MerTK leads to the MerTK tyrosine kinase-dependent assembly of an IKKβ-activation complex, with the involvement of a serine kinase that phosphorylates IKKβ. In this context, we considered a canonical pathway of IKKβ serine phosphorylation involving the adaptor protein MyD88 and the IRAK family of kinases, often referred to as the "Myddosome"[18,29]. Supporting a role for MyD88, we found that treating macrophages with the MyD88 inhibitor TJ-M2010-5[30] blocked AC-induced phosphorylation of IKKβ (Fig. 3a). IRAK1 and IRAK4 are the major IKKβ-activating kinases downstream of MyD88. Consistent with the MyD88 data, ACs induced phosphorylation of IRAK4, which is a measure of its activation (Fig. 3b), and inhibition of IRAK1/4 with KME-2780[31] blocked AC-induced phosphorylation of IKKβ (Fig. 3c). Moreover, immunoprecipitates of MerTK showed AC-induced association with both MyD88 and IRAK4 (Fig. 3d, e). From these data, we propose the following hypothesis: AC-induced activation of MerTK promotes the assembly of MyD88, IRAK4, and IKK, leading to the phosphorylation/activation of IKKβ.

Efferocytosis-induced IKKβ/NFκB/p38 activation promotes multiple pro-resolving pathways

Although IKKβ, NFκB, and p38-STAT3 typically promote inflammatory pathways in macrophages, we wondered whether these upstream signals in the setting of efferocytosis may promote efferocytosis-induced resolution. We first determined whether inhibiting IKKβ or p38-STAT3 signaling could attenuate AC-induced IL-10. IL-10 is a well-known pro-resolving cytokine produced by macrophages during efferocytosis, and it is also transcriptionally induced by both NFκB and p38/STAT3[32–36], but these findings have not previously been linked to efferocytosis. Pre-treatment of mouse BMDMs with IKK16 blocked AC-induced *Il10* mRNA expression, with similar results in HMDMs (Fig. 4a, b). Secreted IL-10 protein in the conditioned media was also increased when BMDMs were incubated with ACs, and this was blocked with IKK16 pre-treatment (Fig. 4c). To complement the IKK16 data, we showed that AC-induced *Il10* was blocked in BMDMs from p65-knockout mice versus control (Ctrl) BMDMs (Fig. 4d). Pre-treatment with the p38 inhibitor SB203580 or the STAT3 inhibitor Stattic[37] also attenuated AC-induced *Il10* (Fig. 4e, f). Stattic, like SB203580 (above), did not affect primary efferocytosis (Supplementary Fig. 3a). Interestingly, efferocytosis-induced *Tgfb1*, which is another mediator that can help mediate tissue resolution[38], was not inhibited by IKK16 treatment (Supplementary Fig. 3b). In contrast, the induction of *Ptgs2*, which is involved in the activation of a PGE_2-mediated efferocytosis-resolution pathway[38], was blocked by inhibiting IKKβ (Supplementary Fig. 3c).

We next assessed whether efferocytosis-induced IKKβ activation promotes the key pro-resolving process of continuing efferocytosis by conducting a sequential double-AC efferocytosis assay[6,17]. Macrophages were pre-treated ± IKK16 before incubation with a first round of PKH67 (green) labeled ACs, chased for 2 h, and then incubated with a second round of PKH26 (red)-labeled ACs. The percentage of green macrophages that were also red, which indicates continuing efferocytosis, was decreased by IKKβ inhibition (Fig. 4g). To determine whether this impairment of continuing efferocytosis by IKKβ inhibition was due to defective AC-binding or AC-internalization, we added the actin polymerization inhibitor cytochalasin D before the addition of the second set of red ACs to block second-AC-internalization but not second-AC-binding[10,11,17,28]. In the presence of cytochalasin D, the percentage of green macrophages that were also red was not decreased by IKKβ inhibition (Fig. 4h), indicating that IKKβ enhances second-AC internalization rather than binding (see Ref[12]. as an example of this approach).

As AC internalization requires the GTPase Rac1[16], we predicted that IKKβ inhibition would lower Rac1 activity after the first round of ACs. Rac1 activity was measured using a bead-phagocytosis assay in which macrophages are first incubated with a round of ACs, followed by a round of beads in the second round rather than ACs[39]. As expected, Rac1 was activated during the second round of phagocytosis in control macrophages, but this activation was attenuated in macrophages pre-treated with IKK16 (Fig. 4i). Finally, given the role of IL-10 in Rac1 activation in macrophages in other settings[39], we hypothesized that IL-10 may be a link between IKKβ activation and continuing efferocytosis. Consistent with this idea, neutralization of the IL-10 receptor after a first round of ACs blocked second AC uptake (Fig. 4j). Thus, the transient activation of IKKβ in primary efferocytosis promotes continuing efferocytosis by activating Rac1 and second-AC internalization, with IKKβ-induced IL-10 contributing to this process.

Another key pro-resolving process is efferocytosis-induced macrophage proliferation (EIMP). EIMP expands the pool of pro-resolving macrophages to enhance AC clearance and tissue repair in vivo[9,13], and recent work has suggested a broad impact of EIMP in many in vivo settings[40–46]. By measuring macrophage cell number following efferocytosis[9,13], we found that inhibition of IKKβ blocked EIMP (Fig. 4k). EIMP is mediated by efferocytosis-induced upregulation of Myc, and we found that IKK16 blunted the increase in Myc in efferocytosing macrophages (Fig. 4l). We also found that treatment of macrophages with inhibitors of NFκB (helenalin[47]), p38 (SB203580), or

https://doi.org/10.1038/s41467-026-78229-x

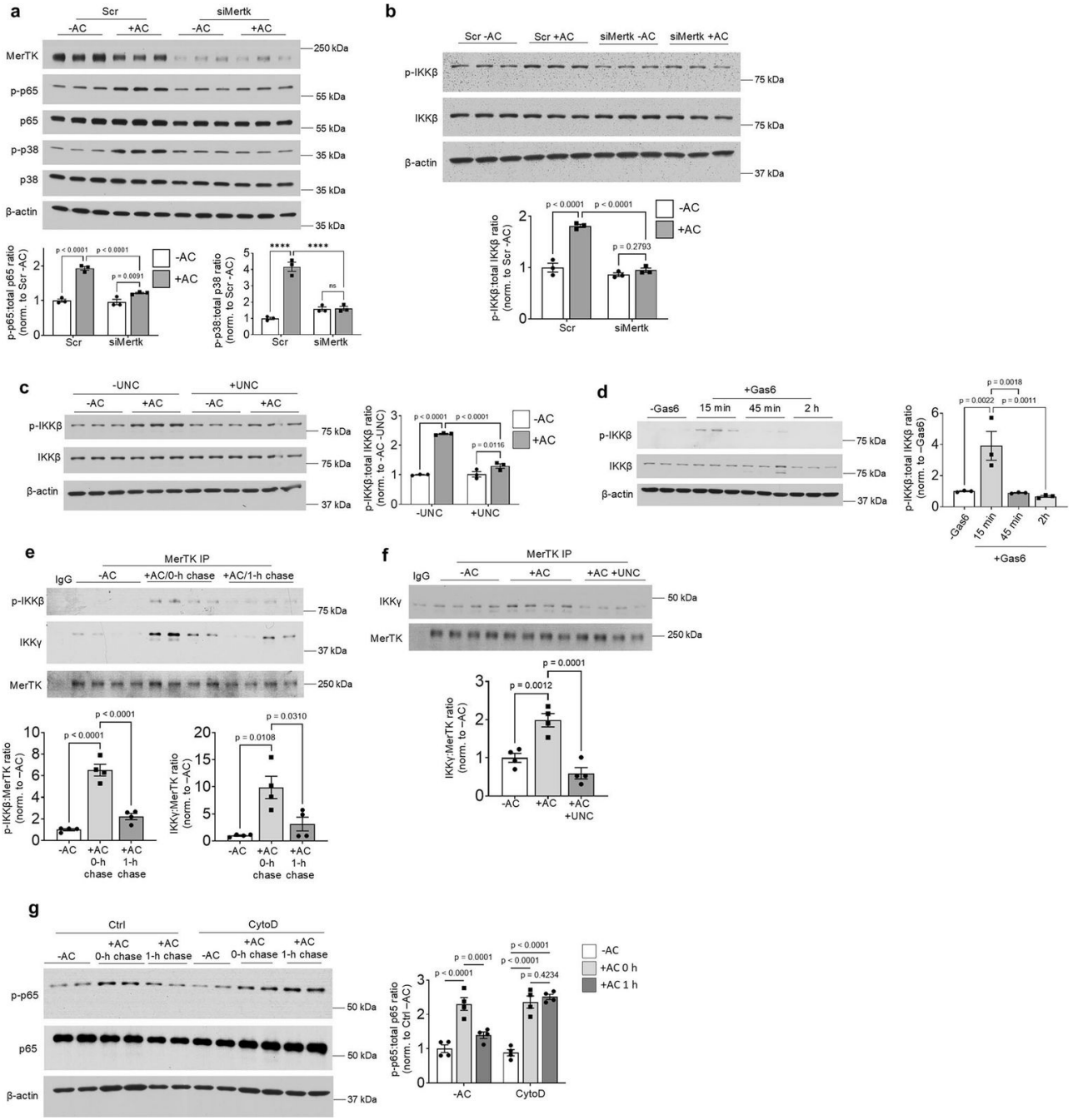


Fig. 2 | MerTK activation by ACs triggers IKK-NFκB/p38 signaling in macrophages. a BMDMs transfected with scrambled or siMertk were incubated ± ACs for 45 min and immunoblotted for phospho- and total p65 and p38 ($n = 3$). **b** As in a, but the cells were immunoblotted for phospho-IKKβ and total IKKβ ($n = 3$). **c** BMDMs were pre-treated with 1 μM UNC5293 (UNC, MerTK kinase inhibitor) for 2 h and incubated ± ACs for 45 min and immunoblotted for phospho-IKKβ and total IKKβ ($n = 3$). **d** BMDMs were incubated with Gas6-conditioned media for the indicated periods and immunoblotted for phospho-IKKβ and total IKKβ ($n = 3$). **e** BMDMs were incubated ± ACs for 45 min and harvested (0-h chase) or chased for 1 h. Cell lysates were immunoprecipitated (IP) with IgG or anti-MerTK antibody and immunoblotted for phospho-IKKβ, IKKγ, and MerTK. Phospho-IKKβ and IKKγ were quantified relative to MerTK expression and normalized to the -AC group ($n = 4$). **f** BMDMs pre-treated for 2 h ± 1 μM UNC5293 (UNC) were incubated ± ACs for 45 min. Cell lysates were immunoprecipitated (IP) with IgG or anti-MerTK antibody and immunoblotted for IKKγ and MerTK. IKKγ was quantified relative to MerTK expression and normalized to the -AC group ($n = 4$). **g** BMDMs were pre-treated for 20 min ± 5 μM cytochalasin D (CytoD) and incubated ± ACs for 45 min. The cells were then harvested (0-h chase) or chased for 1 h and immunoblotted and quantified for p-p65 and total p65 ($n = 4$). The immunoblot illustrates the results for 2 of the 4 lysates for each group. The densitometric ratio data are normalized to the first control group in each experiment. Bars represent means ± SEM. Statistics were performed using a one-way ANOVA for **d**–**f**, two-way ANOVA for (**a**–**c**, **g**).

STAT3 (Stattic) blocked efferocytosis-induced Myc (Supplementary Fig. 3d–f). However, Myc was not downstream of IL-10, as IL-10 receptor neutralization did not block the efferocytosis-induced upregulation of Myc (Supplementary Fig. 3g). These data show that the IKKβ-mediated NFκB and p38-STAT3 pathways in efferocytosing macrophages play key roles in three interconnected downstream pro-resolving processes: induction of IL-10, continuing efferocytosis, and Myc-mediated EIMP.

https://doi.org/10.1038/s41467-026-78229-x

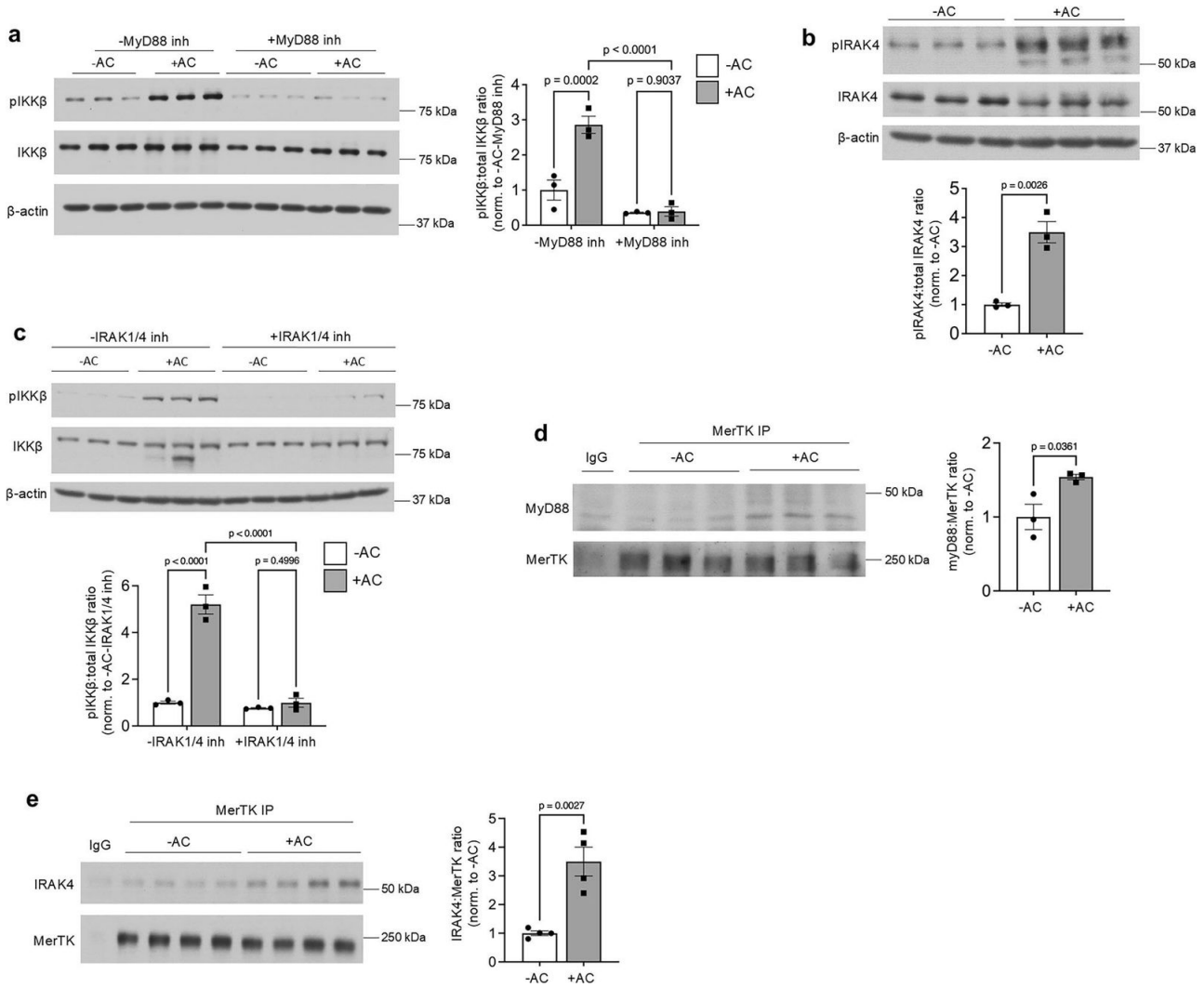


Fig. 3 | MerTK-mediated activation of the IKKβ pathway involves MyD88 and IRAK4. a BMDMs were pre-treated with 25 μM of the MyD88 inhibitor TJ-M2010-5 for 2 h and incubated ± ACs for 45 min and then immunoblotted for phospho-IKKβ and total IKKβ ($n = 3$). **b** BMDMs were incubated ± ACs for 45 min and then immunoblotted for phospo-IRAK4 and total IRAK4 ($n = 3$). **c** BMDMs were pre-treated with 1 μM IRAK1/4 inhibitor for 2 h and incubated ± ACs for 45 min and then immunoblotted for phospho-IKKβ and total IKKβ ($n = 3$). **d** BMDMs were incubated ± ACs for 45 min. Cell lysates were immunoprecipitated (IP) with IgG or anti-MerTK antibody and immunoblotted for MyD88 and MerTK. MyD88 was quantified relative to MerTK expression and normalized to the -AC group ($n = 3$). **e** BMDMs were incubated ± ACs for 45 min. Cell lysates were immunoprecipitated (IP) with IgG or anti-MerTK antibody and immunoblotted for IRAK4 and MerTK. IRAK4 was quantified relative to MerTK expression and normalized to the -AC group ($n = 4$). The densitometric ratio data are normalized to the first control group in each experiment. Bars represent means ± SEM. Statistics were performed using two-way ANOVA for **a**, **c** and Student's *t*-test in (**b**, **d**, and **e**).

A fourth pro-resolving endpoint of efferocytosis-induced IKKβ/NFκB/p38

We became interested in a cell-surface molecule called PD-L1, which has roles in the suppression of immunity in cancer[21,48] and the development of regulatory T cells (T_{reg}) cells[49], which can enhance macrophage efferocytosis and tissue resolution[39,50]. Moreover, a recent in vitro study showed that exposure of RAW264.7 cells to apoptotic osteosarcoma cells increased PD-L1 expression in a MerTK/p38-dependent manner[21]. However, the mechanism and relevance to efferocytosis-induced resolution in vivo remain unknown. We began by asking if PD-L1 might be part of a pro-resolving pathway downstream of IKKβ in efferocytosing macrophages. We found that *Cd274* mRNA (gene name for PD-L1) was markedly increased in efferocytosing macrophages (Fig. 5a). Furthermore, cell-surface PD-L1 protein was increased in efferocytosing macrophages compared with non-efferocytosing macrophages, and this increase was blocked by a MerTK-neutralizing antibody (Fig. 5b). Critically, efferocytosis-induced *Cd274/CD274* mRNA was decreased when mouse or human macrophages were exposed to IKK16 or in p65-knockout BMDMs (Fig. 5c, d). Moreover, AC-induced *Cd274* induction was also blunted by inhibitors of p38 and STAT3, and si*Myc* (Fig. 5e–g).

We next explored whether efferocytosis-induced PD-L1 was involved in pro-resolving macrophage reprogramming, beginning with continuing efferocytosis. We found that silencing PD-L1 impaired continuing efferocytosis but not primary efferocytosis (Fig. 5h and Supplementary Fig. 4a, b). Similarly, PD-L1 het-KO BMDMs (*Cd274*$^{fl/+}$; *LysMCre*$^{+/-}$) also displayed a reduction in continuing efferocytosis compared with control macrophages (Fig. 5i). The impairment of continuing efferocytosis with PD-L1 silencing was not observed in cytochalasin D-treated macrophages (Fig. 5j), indicating impaired second-AC internalization. In line with this finding, PD-L1 deficiency attenuated Rac1 activation during the second round of phagocytosis (Fig. 5k). Thus, PD-L1 represents another factor downstream of IKKβ that contributes to Rac1 activation and continuing efferocytosis.

The above data indicated that Myc was upstream of *Cd274* induction in efferocytosing macrophages, but further work suggested

https://doi.org/10.1038/s41467-026-78229-x

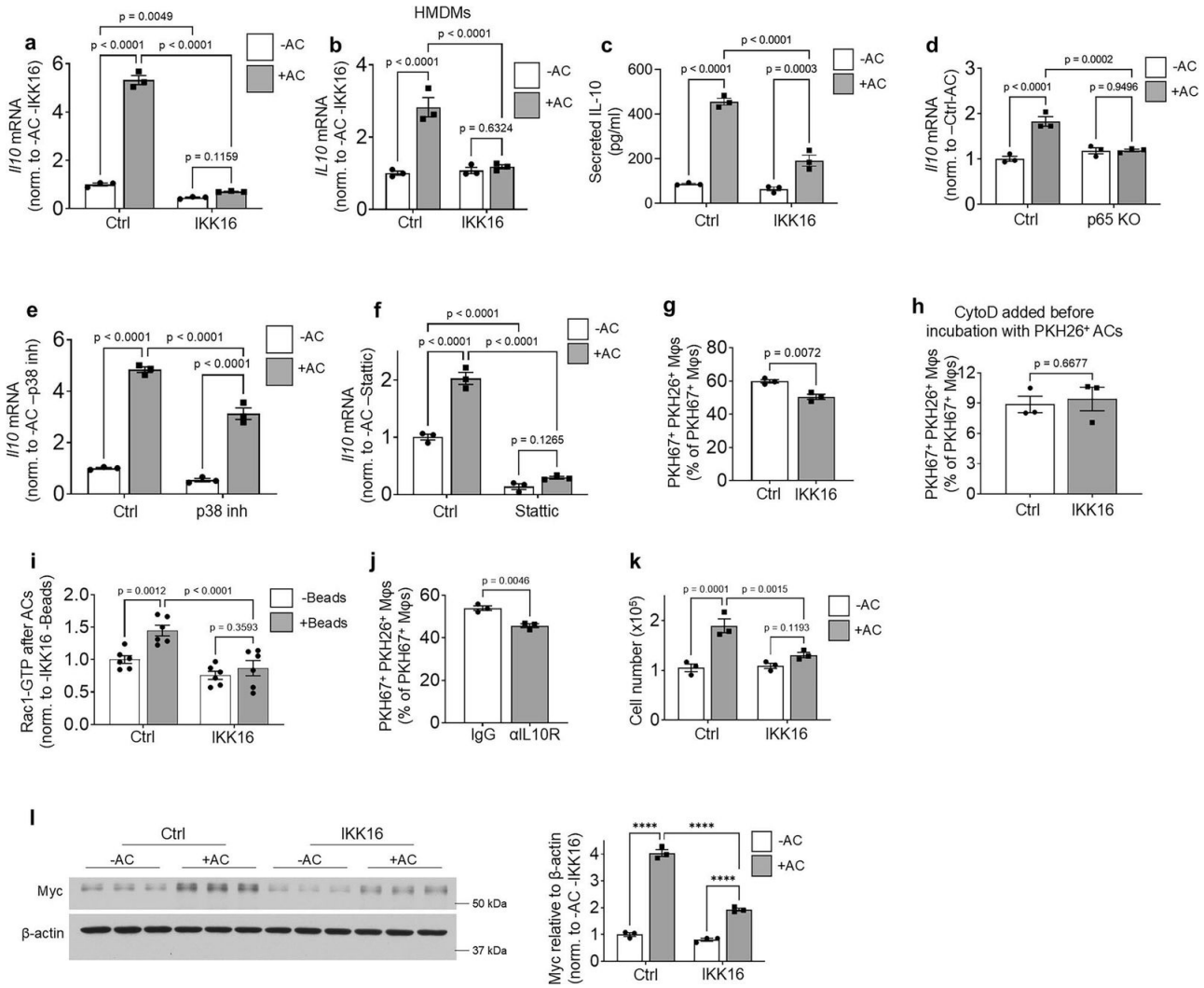


Fig. 4 | The efferocytosis-IKK pathway contributes to IL-10 induction, continuing efferocytosis, and macrophage proliferation. **a** BMDMs pre-treated for 2 h with vehicle control (Ctrl) or IKK16 were incubated ± ACs for 45 min, chased for 1 h, and assayed for *Il10* mRNA ($n = 3$). **b** As in panel a but with HMDMs ($n = 3$). **c** BMDMs were pre-treated with vehicle control or IKK16 for 2 h, incubated ± ACs for 45 min, and chased for 4 h. Conditioned media were and assayed for secreted IL-10 by ELISA ($n = 3$). **d** Control and p65-knockout BMDMs were treated ± ACs for 45 min, chased for 1 h, and assayed for *Il10* mRNA ($n = 3$). **e**, **f** BMDMs pre-treated for 2 h with vehicle control or 10 μM p38 inhibitor or 2.5 μM Stattic were incubated ± ACs for 45 min, chased for 1 h, and assayed for *Il10* mRNA ($n = 3$). **g** BMDMs pre-treated with vehicle control or IKK16 for 2 h were incubated with PKH67-labeled ACs (green) for 45 min, chased for 2 h, and incubated with PKH26-labeled ACs (red) for 45 min. The percentage of PKH67$^+$ BMDMs that were also PKH26$^+$ ($n = 3$) was quantified by fluorescence microscopy. **h** As in **g**, but the macrophages were treated with 5 μm cytochalasin D 20 min before the addition of the PKH26-labeled ACs ($n = 3$). **i** BMDMs pre-treated for 2 h with vehicle control or IKK16 were incubated with ACs for 45 min, chased for 2 h, incubated ± beads for 20 min, and assayed for Rac1 activity ($n = 6$). **j** BMDMs pre-treated with IgG or anti-IL-10R were assayed as in g ($n = 3$). **k** BMDMs pre-treated with vehicle control or IKK16 for 2 h were incubated ± ACs for 45 min, chased for 24 h, and quantified for cell number ($n = 3$). **l** BMDMs pre-treated for 2 h with vehicle control or IKK16 for 2 h were incubated ± ACs for 45 min, chased for 3 h, and immunoblotted for Myc ($n = 3$). Bars represent means ± SEM. Statistics were performed using the Student's *t*-test in **g**, **h**, **j** and two-way ANOVA in **a**–**f**, **i**, **k**, **l**.

an intermediary process between Myc and increased *Cd274* mRNA. In this context, we looked into a possible role for the DNA demethylase TET2. Although not previously implicated in efferocytosis, Myc has been linked to TET2 expression in rat heart tissue[51], and Tet1-induced DNA demethylation increases *Cd274* expression in human macrophages[52]. We found that *Tet2* mRNA both in BMDMs and HMDMs and TET2 protein in BMDMs were upregulated in efferocytosing macrophages, which was blocked by IKK16 (Fig. 6a, b). The AC-induced increase in *Tet2* mRNA was also impaired in p65-knockout BMDMs, further validating TET2 as a key downstream player induced by transient activation of IKKβ/NF-κB pathway (Fig. 6c). Efferocytosis-induced *Tet2* mRNA was also dependent on p38, STAT3, and Myc (Fig. 6d–f and Supplementary Fig. 4c). Most importantly, efferocytosis-induced upregulation of *Cd274* was blunted in TET2-knockout macrophages (Fig. 6g), despite no change in primary efferocytosis (Supplementary Fig. 4d). The greater effect of siMyc versus TET2 KO in preventing AC-induced *Cd274* mRNA may suggest that other factors downstream of Myc are also involved. In summary, in addition to the pro-resolving endpoints elucidated in the previous section, the findings here suggest another endpoint involving a Myc-TET2-PD-L1 pathway.

In vivo evidence that efferocytosis-induced IKKβ promotes tissue repair

To test the role of efferocytosis-induced IKKβ in tissue repair, we transplanted recipient mice with bone marrow from *Ikbkb*$^{fl/fl}$ control (Ctrl) mice or *Ikbkb*$^{fl/fl}$;*Cx3cr1*$^{CreERT2/+}$ mice to enable tamoxifen-inducible knockdown (KD) of IKKβ in macrophages. The mice were injected with tamoxifen before DEX injection to lower macrophage IKKβ expression

https://doi.org/10.1038/s41467-026-78229-x

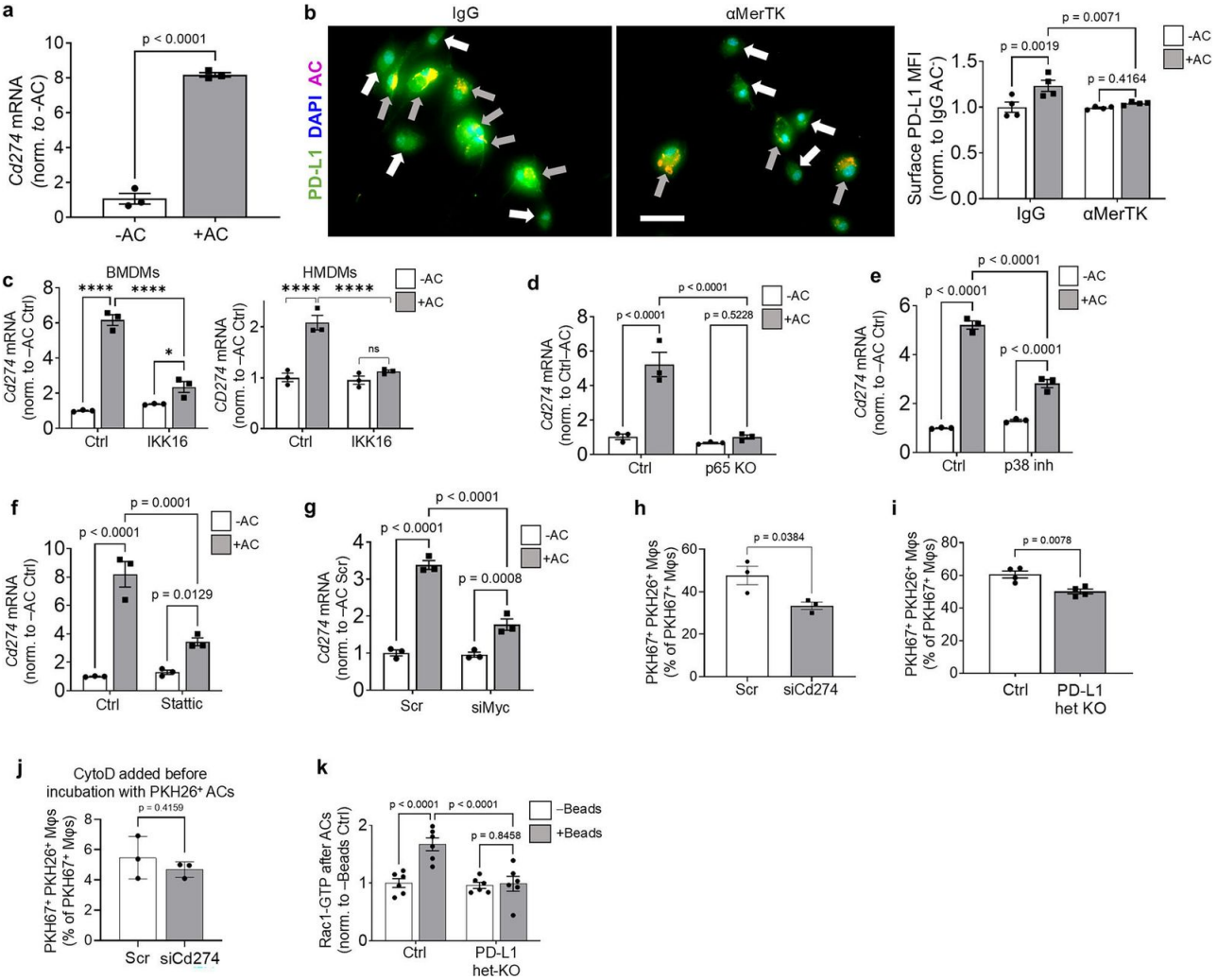


Fig. 5 | The efferocytosis-IKKβ pathway induces PD-L1, which contributes to continuing efferocytosis. a BMDMs were incubated ± ACs for 45 min, chased for 6 h, and assayed for *Cd274* (PD-L1) mRNA ($n = 3$). **b** BMDMs pre-treated with IgG or anti-MerTK for 2 h were incubated with PKH26-labeled ACs for 45 min, chased for 6 h, subjected to non-permeabilizing immunostaining for cell-surface PD-L1, and imaged by confocal microscopy ($n = 4$). Scale bar, 20 µm. **c** BMDMs or HMDMs pre-treated for 2 h with vehicle control or IKK16 were incubated ± ACs for 45 min, chased for 6 h, and assayed for *Cd274* or *CD274* mRNA ($n = 3$). **d** Control and p65-knockout BMDMs were incubated ± ACs for 45 min, chased for 6 h, and assayed for *Cd274* mRNA ($n = 3$). **e**, **f** BMDMs pre-treated for 2 h with vehicle control (Ctrl), 10 µM SB203580 (p38 inh), or 2.5 µM Stattic were incubated ± ACs for 45 min, chased for 6 h, and assayed for *Cd274* mRNA ($n = 3$). **g** BMDMs transfected with 50 nM scrambled RNA or siMyc were incubated ± ACs for 45 min, chased for 6 h, and assayed for *Cd274* mRNA ($n = 3$). **h** BMDMs transfected with 50 nM scrambled or siCd274, or **i** $Cd274^{fl/+}$(Ctrl) and $Cd274^{fl/+}$;$LysMCre^{+/-}$ (PD-L1-het KO) BMDMs, were incubated with PKH67-labeled ACs for 45 min, chased for 2 h, and incubated with PKH26-labeled ACs for 45 min. The images were quantified for the percentage of $PKH67^+$ BMDMs that were also $PKH26^+$ ($n = 3$). **j** As in **i**, but the macrophages were treated with 5 µm cytochalasin D 20 min before the addition of the PKH26-labeled ACs ($n = 3$). **k** The macrophages in **i** were incubated with ACs for 45 min, chased for 2 h, incubated with 6–8 µm polystyrene beads for 20 min, and assayed for Rac1 activity ($n = 6$). Bars represent means ± SEM. Statistics were performed using the Student's *t*-test for **a**, **h**–**j** and two-way ANOVA for (**b**–**g**, **k**).

in the $Ikbkb^{fl/fl}$;$Cx3cr1^{CreERT2/+}$ cohort. The thymi were then analyzed 18 h after DEX injection, which is the time point when the pro-resolving effects of efferocytosis in the thymus become apparent[10,17]. Compared with the IKKβ Ctrl group, we achieved ~70% lowering of macrophage IKKβ expression in the Mφ-IKKβ-KD group (Fig. 7a). To measure efferocytosis, thymi are immunostained for Mac2 or CD68 to identify macrophages and stained with TUNEL (TUN) to identify ACs, followed by the quantification of the ratio of TUN^+ cells that co-localize with the cytoplasm of $Mac2^+$/$CD68^+$ cells ($cTUN^+$) to free TUN^+ cells[10,17]. In the DEX-thymus model where there is a high ratio of apoptotic thymocytes to thymic macrophages, this assay primarily measures continuing efferocytosis[10,17]. By this measure, continuing efferocytosis was impaired in the Mφ-IKKβ-KD cohort, whereas the total number of thymic macrophages was similar between the two groups (Fig. 7b). Moreover, H&E staining of the thymus revealed more necrosis in Mφ-IKKβ-KD versus control thymi, suggesting increased secondary necrosis from uncleared ACs and impaired tissue repair[10,17] (Fig. 7c). The thymic macrophages in the Mφ-IKKβ-KD cohort also had reduced expression of IL-10 (Fig. 7d).

To explore efferocytosis-induced PD-L1 in vivo, we returned to the DEX-thymus model and found that the thymi of control DEX-injected mice had significantly higher PD-L1 expression in $cTUN^+$ efferocytosing $F4/80^+$ macrophages compared to thymi from control PBS-injected mice (Fig. 7e). Importantly, this increase in PD-L1 expression in efferocytosing thymic macrophages was lower in the thymi of Mφ-IKKβ-KD mice (Fig. 7f). We next focused on the role of Myc-TET2 in this model. Analysis of the thymi from the DEX-treated Ctrl and Mφ-IKKβ-KD mice revealed that efferocytosing macrophages in the Ctrl group had both elevated Myc and TET2 compared with non-efferocytosing macrophages, whereas there was no increase in Myc or TET2 in

https://doi.org/10.1038/s41467-026-78229-x

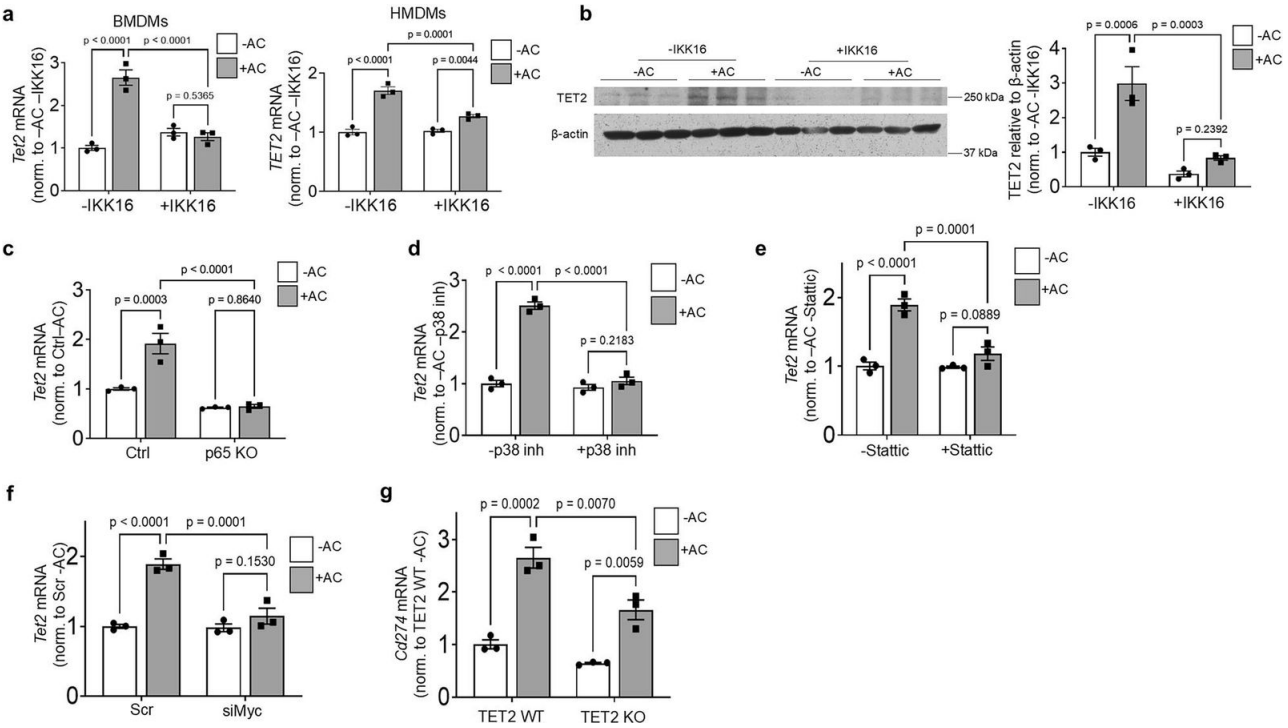


Fig. 6 | The IKKβ pathway induces PD-L1 via Myc and TET2. a, **b** BMDMs and HMDMs pre-treated for 2 h with vehicle control or IKK16 were incubated ± ACs for 45 min, chased for 6 h, and assayed for *Tet2* or *TET2* mRNA or immunoblotted for TET2 protein (BMDMs, $n = 3$). **c** Control and p65 KO BMDMs were incubated ± ACs for 45 min, chased for 6 h, and assayed for *Tet2* mRNA ($n = 3$). **d**, **e** BMDMs pre-treated for 2 h with vehicle control (Ctrl), 10 μM SB203580 (p38 inh), or 2.5 μM Stattic were incubated ± ACs for 45 min, chased for 6 h, and assayed for *Tet2* mRNA ($n = 3$). **f** BMDMs transfected with 50 nM scrambled or siMyc for 72 h were incubated ± ACs for 45 min, chased for 6 h, and assayed for *Tet2* mRNA. **g** WT or TET2-KO BMDMs were incubated ± ACs for 45 min, chased for 6 h, and assayed for *Cd274* mRNA ($n = 3$). Bars represent means ± SEM. Statistics were performed using two-way ANOVA (**a**–**g**).

efferocytosing macrophages in the Mφ-IKKβ-KD group (Fig. 8a, b). We then conducted a DEX-thymus experiment using mice transplanted with bone marrow from WT or TET2 KO mice. In the TET2 KO group, we verified the knockdown of TET2 in Mac2$^+$ thymic macrophages (Supplementary Fig. 4e). We showed that efferocytosing thymic macrophages in the WT cohort, but not the TET2-KO cohort, had elevated PD-L1 expression versus non-efferocytosing macrophage (Fig. 8c). Moreover, the ratio of macrophage-associated to free ACs was lower in the TET2-KO thymus (Fig. 8d). Importantly, thymic necrosis was increased in the KO cohort, suggesting impaired tissue repair (Fig. 8e). These changes occurred without significant differences in the circulating immune cell numbers (Supplementary Fig. 4f–k).

To examine the consequences of macrophage PD-L1 deficiency in vivo, we conducted a DEX-thymus experiment using mice transplanted with bone marrow from *Cd274*$^{fl/+}$ (control) or *Cd274*$^{fl/+}$;*LysMCre*$^{+/-}$ (PD-L1 het-KO) mice. Macrophages in the thymi of PD-L1 het-KO mice displayed a reduced ratio of macrophage associated to free ACs and increased thymic necrosis (Fig. 8f,g). Given a possible link to T_{reg} cells (above), we immunostained the thymi of control and PD-L1 het-KO mice for FoxP3, a master transcriptional regulator and marker of T_{reg} cells, and found that the thymi from the PD-L1 het-KO mice had reduced T_{reg} cell content compared with control thymi (Fig. 8h), with no change in the total number of thymic cells between the two groups (Supplementary Fig. 5a). These defects in the PD-L1 het-KO mice were observed without any significant difference in circulating immune cell numbers (Supplementary Fig. 5b–g). Thus, PD-L1 is a key downstream mediator of the IKKβ-Myc-TET2 resolution pathway in efferocytosing macrophages. In summary, the efferocytosis-IKKβ pathway, by promoting IL-10/PD-L1-induced continuing efferocytosis, Myc-induced EIMP, and PD-L1-induced T_{reg} cells, enhances an integrated, multipronged program of efferocytosis-induced tissue resolution (Fig. 8i).

Inducible deletion of macrophage IKKβ during atherosclerosis regression prevents lesional fibrous cap thickening

A critically important role of the efferocytosis-resolution cycle in humans and experimental models is facilitating tissue repair in the arterial wall during a process called atherosclerosis regression, which is induced by the lowering of plasma low-density lipoprotein (LDL) cholesterol[2,50,53]. In humans and mice, LDL-lowering promotes the thickening of a protective fibrous cap over atherosclerotic lesions, which in humans is associated with a decreased incidence of plaque rupture and acute cardiovascular events such as myocardial infarction[53–55]. Moreover, in regressing plaques, there are increases in efferocytosis, T_{reg} cells, and pro-resolving molecules, all of which contribute to the beneficial changes in plaque morphology[17,39,50,56]. To test the role of efferocytosis-induced activation of IKKβ in this process, we transplanted *Ldlr*$^{-/-}$ mice with bone marrow cells from control *Ikbkb*$^{fl/fl}$ or *Ikbkb*$^{fl/fl}$;*Cx3cr1*$^{CreERT2/+}$ (Mφ-IKKβ-KD) mice and then fed the mice a high-fat, high-cholesterol Western-type diet for 16 weeks to induce atherosclerosis (baseline). Regression was then induced by restoring LDL receptor expression in the liver and switching to a chow diet. At the same time, all regression mice received tamoxifen injections twice a week for 7 weeks to knockdown macrophage IKKβ in the *Ikbkb*$^{fl/fl}$;*Cx3cr1*$^{CreERT2/+}$ group. As designed, the regression protocol caused a marked reduction in plasma cholesterol and a modest decline in body weight and fasting blood glucose in both regression groups (Supplementary Fig. 6a–c). The regression groups also had a few differences in the differential blood cell count compared with the baseline group. However, these parameters were statistically similar in the control and Mφ-IKKβ-KD cohorts, except for the blood neutrophil count, which was slightly higher in the KD group (Supplementary Fig. 6d–j). We then confirmed that macrophage IKKβ was lower in the regressing lesions of the Mφ-IKKβ-KD mice versus the regressing

https://doi.org/10.1038/s41467-026-78229-x

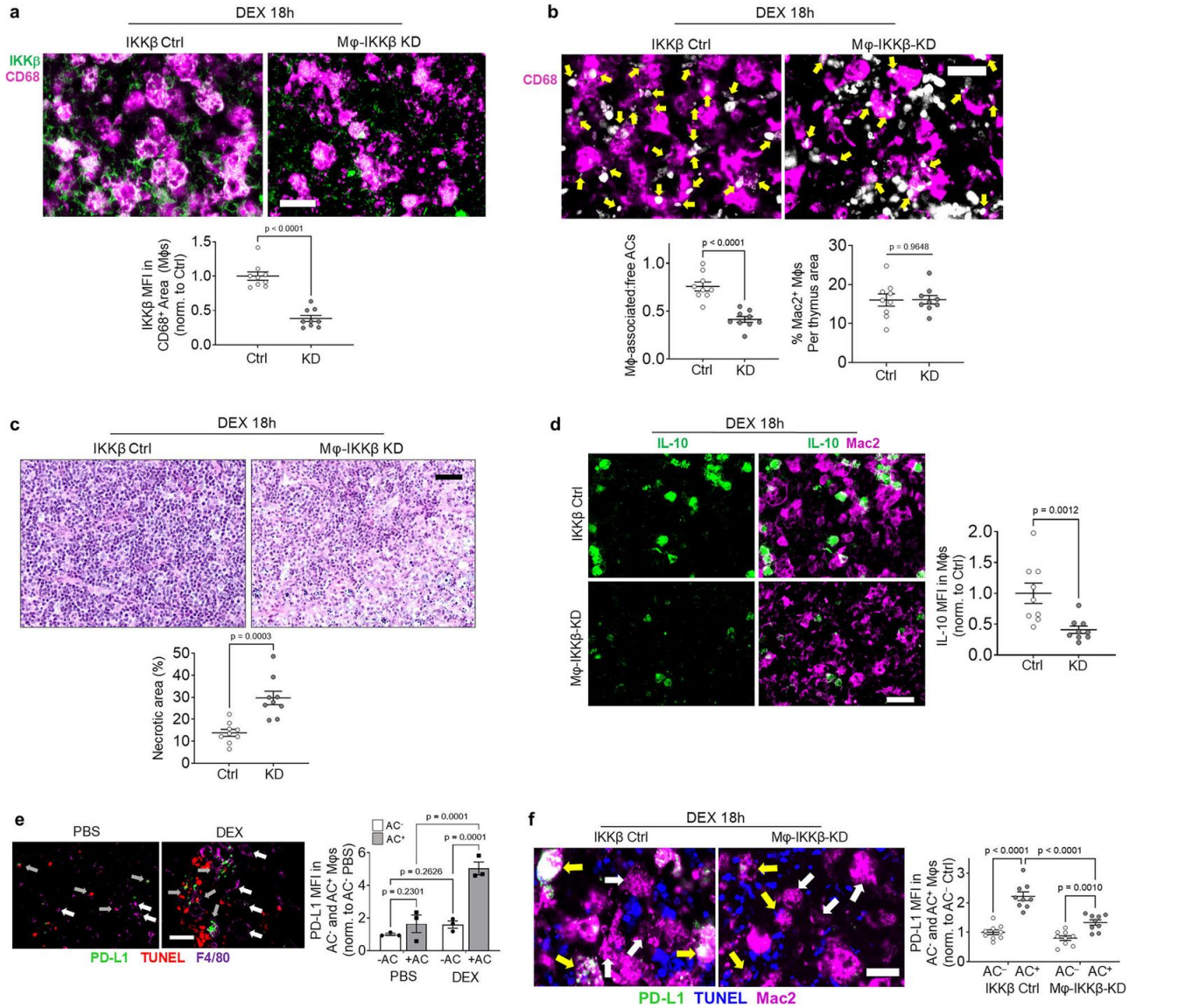
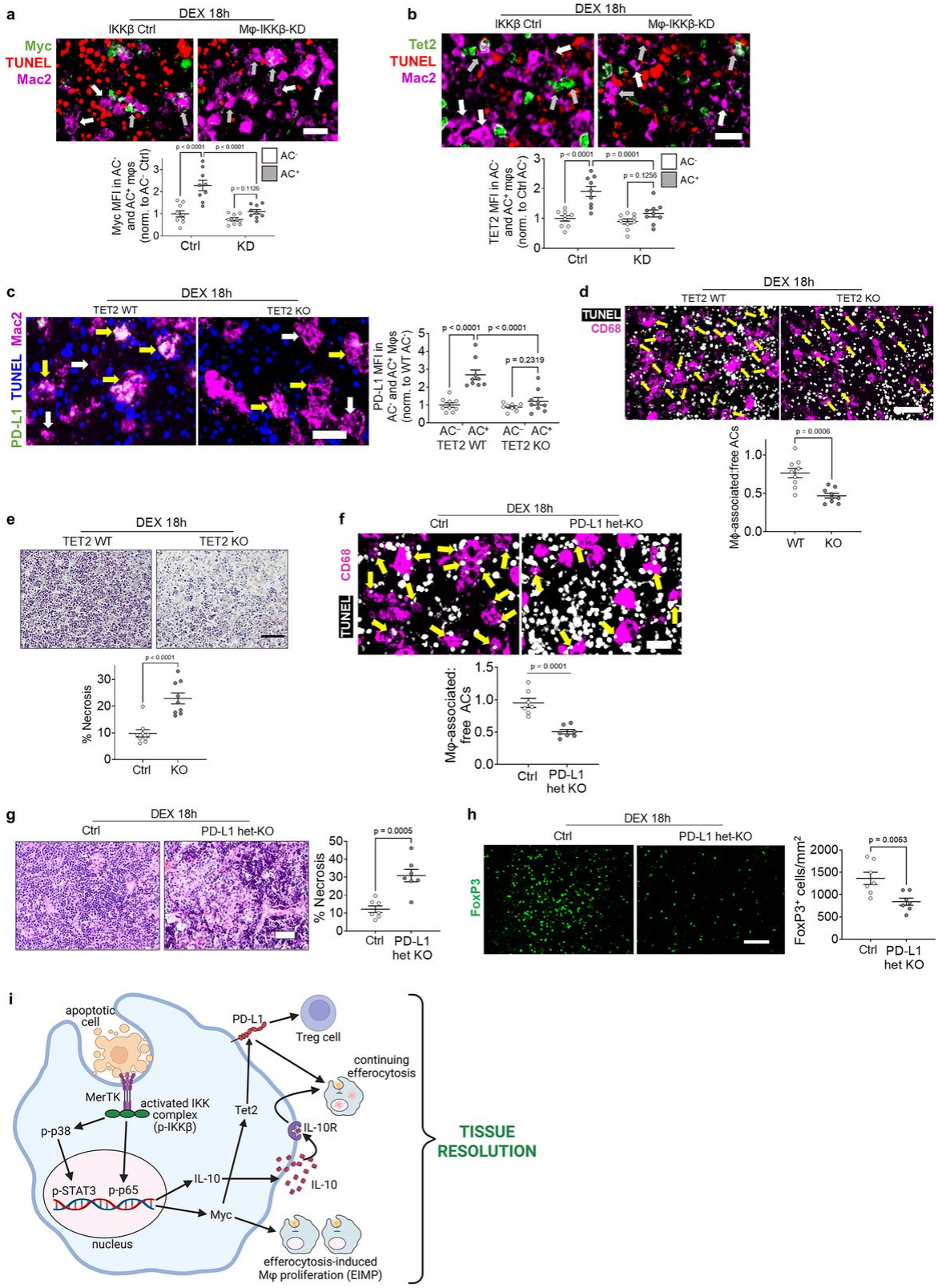


Fig. 7 | In vivo evidence linking IKK to continuing efferocytosis, IL-10, and PD-L1. Mice were transplanted with *Ikbkb*$^{fl/fl}$ (IKKβ Ctrl) or *Ikbkb*$^{fl/fl}$;*Cx3cr1*$^{CreERT2/+}$ (Mφ-IKKβ-KD [knockdown]) bone marrow, treated with tamoxifen daily for 5 days, and then injected with DEX. Thymus sections from these mice were assayed 18 h later ($n = 9$ mice per group). **a** Sections were immunostained for IKKβ and CD68. IKKβ MFI in CD68$^+$ was quantified and normalized to the Ctrl group. Scale bar, 25 μm. **b** Sections were labeled with TUNEL, immunostained for Mac2, and quantified for the ratio of TUNEL$^+$ cells that localize to the cytoplasm of CD68$^+$ cells (macrophage-associated ACs) to free TUNEL$^+$ cells (free ACs). Yellow arrows indicate macrophage-associated ACs. Scale bar, 20 μm. Also shown are the total number of Mac2+ macrophages per thymic area. **c** Sections were stained with H&E and quantified for the percent necrotic area, identified by regions of hypocellularity and small, fragmented nuclei. Scale bar, 50 μm. **d** Sections were immunostained for Mac2 and IL-10, and the MFI of IL-10 in Mac2$^+$ cells was quantified and normalized to the Ctrl group. Scale bar, 20 μm. **e** Mice were injected with PBS or DEX and, after 18 h, the thymic sections were labeled with TUNEL and immunostained for F4/80 and PD-L1, followed by imaging and quantification of PD-L1 MFI in cTUN$^-$ or cTUN$^+$ F4/80$^+$ macrophages ($n = 3$). Scale bar, 20 μm. **f** Similar to **e**, but the mice were either IKKβ Ctrl or Mφ-IKKβ-KD, and thymic sections immunostained for Mac2 to identify macrophages ($n = 9$). Scale bar, 20 μm. Bars represent means ± SEM. Statistics were performed using the Student's *t*-test for **a**–**d** and two-way ANOVA for (**e**, **f**).

lesions of the control mice (Fig. 9a). Most importantly, the regression-induced increase in fibrous cap thickness seen in the control regression lesions was attenuated in the Mφ-IKKβ-KD regressing lesions (Fig. 9b). This difference occurred despite no significant changes in lesional or necrotic area (Supplementary Fig. 6k, l). Although the KD group had a modest increase in circulating neutrophils (above), a subgroup analysis of the majority of mice with similar neutrophil counts demonstrated the same effect of Mφ-IKKβ-KD on cap thickness (Supplementary Fig. 6m, n).

As mentioned above, another key endpoint in regression is efferocytosis by lesional macrophages, which primarily reflects the process of continuing efferocytosis[17,50]. As expected, regression caused an increase in the ratio of macrophage-associated to free ACs, and we now show that lesional efferocytosis was blunted in the Mφ-IKKβ-KD cohort (Fig. 9c). Lesional macrophage content was lower in regression versus baseline as expected[57], but the two regression groups had similar macrophage content (Supplementary Fig. 6o). Another key pro-resolving mediator in the pathway, IL-10, was increased in control regressing lesional macrophages compared with baseline, but its expression was decreased in Mφ-IKKβ-KD versus control regressing lesions (Fig. 9d). Moreover, the expression levels of Myc and the percent Ki67 positivity were increased in AC$^+$ (efferocytosing) macrophages in control regressing lesions compared with the following: (1) baseline lesional macrophages; (2) AC$^-$ macrophages

https://doi.org/10.1038/s41467-026-78229-x



in control regressing lesions; and (3) and both AC$^+$ and AC$^-$ macrophages in Mφ-IKKβ-KD regressing lesions (Fig. 9e, f). These data are consistent with a role for macrophage IKKβ in EIMP during regression[9]. Two other markers of the IKKβ pathway, TET2 and PD-L1, were also elevated in efferocytosing macrophages in the regressing lesions of control but not Mφ-IKKβ-KD mice (Fig. 9g, h). Finally, we assayed the lesions for FoxP3$^+$ cells as a marker of T_{reg} cells. As predicted, FoxP3$^+$ cells were increased in control regressing versus baseline lesions[50]. However, the regressing lesions of Mφ-IKKβ-KD mice showed a blunted increase in FoxP3$^+$ cells (Fig. 9i). In contrast, the percentage of total CD3$^+$ T cells among all DAPI$^+$ lesional cells was decreased in both regression groups relative to baseline, but there was no difference in

Fig. 8 | In vivo evidence for the pro-resolving roles of TET2 and PD-L1. **a**, **b** Thymus sections from the IKKβ Ctrl and Mφ-IKKβ-KD DEX-thymus mice in Fig. 7 were labeled with TUNEL and immunostained for Mac2 and Myc or TET2. The images were quantified for Myc and TET2 MFI in $Mac2^+$ cells that were $cTUN^-$ (AC^-) or $cTUN^+$ (AC^+), normalized to the Ctrl AC^- group ($n = 9$). Scale bar, 20 μm. **c**–**e** Similar to panel a, but the mice were transplanted with WT or TET2-KO BM cells. **c** Thymic sections were labeled with TUNEL and immunostained for Mac2 and PD-L1, followed by imaging and quantification of PD-L1 MFI in $cTUN^-$ or $cTUN^+$ $Mac2^+$ cells ($n = 3$). Scale bar, 20 μm. **d** Thymic sections were stained with TUNEL, immunostained for CD68, and quantified for the ratio of CD68-associated $TUNEL^+$ cells to free $TUNEL^+$ cells. Scale bar, 40 μm. **e** H&E-stained thymus sections were quantified for the percent necrotic area. Scale bar, 100 μm. **f**–**h** Mice transplanted with *Cd274*$^{fl/+}$ (Ctrl) or *Cd274*$^{fl/+}$*;LysMCre*$^{+/-}$ (PD-L1-Het) bone marrow cells were injected with DEX, and, after 18 h, the thymic sections were analyzed. **f** The sections were labeled with TUNEL and immunostained for CD68 to quantify the ratio of macrophage-associated $TUNEL^+$ cells (arrows) to free $TUNEL^+$ cells ($n = 7$). Scale bar, 20 μm. **g** The sections were H&E-stained and assayed for the percent necrotic area ($n = 7$). Scale bar, 50 μm. **h** The sections were immunostained for FoxP3 and quantified for the number of $FoxP3^+$ cells/mm^2 ($n = 7$). Scale bar, 75 μm. **i** Summary schematic of the proposed pathway. ACs rapidly and transiently activate a MerTK/IKKβ pathway, leading to the activation of NFκB (p-p65) and p38-STAT3 signaling. Nuclear p-p65 and p-STAT3 induce IL-10 and Myc. IL-10 promotes continuing efferocytosis. Myc induces TET2, which leads to increased PD-L1 expression. PD-L1 works with IL-10 to enhance continuing efferocytosis and also promotes the development of T_{reg} cells. Collectively, these processes facilitate tissue resolution. The image was created in BioRender. Tabas, I. (2026). https://BioRender.com/vz0n3k5. Bars represent means ± SEM. Statistics were performed using the Student's *t*-test for **d**–**h** and two-way ANOVA for (**a**–**c**).

lesional $CD3^+$ cells between control and Mφ-IKKβ-KD in the regression groups (Supplementary Fig. 6p). These combined data provide evidence for the pro-resolving role of the efferocytosis-IKKβ pathway in atherosclerosis regression.

Discussion

The findings in this report identify a common upstream pathway in efferocytosing macrophages that triggers multiple downstream resolution processes. In our studies on how efferocytosis reprograms macrophages to a pro-resolving state, the process described here is the earliest pathway we have identified thus far, occurring as soon as 15 min after macrophages are exposed to ACs. For this pathway, efferocytosing macrophages appear to have used signaling molecules that typically activate inflammatory pathways in macrophages. Ironically, some of these pathways are suppressed by efferocytosis in inflammatory macrophages. For example, efferocytosis lowers NFκB activity in macrophages and dendritic cells exposed to high-dose lipopolysaccharide (LPS)[58,59]. The transient nature of IKKβ activation in efferocytosing macrophages versus the more prolonged activation in inflammatory macrophages is probably a key determinant of its net pro-resolving effect. Our data suggest that the MerTK receptor promotes the assembly of the canonical Myddosome and IKK complex in efferocytosing macrophages, while IKK complex formation in inflammatory macrophages is usually downstream of toll-like receptor or cytokine receptor activation[20]. While further work is needed to understand how MerTK leads to assembly of the Myddosome, including the role of the tyrosine kinase activity of MerTK, this difference in receptor involvement may contribute to the transient nature of the signal during efferocytosis. For example, phagosomes containing efferocytosis receptors are internalized by an actin-dependent process soon after ACs bind to these receptors[16], and this process may deactivate the MerTK-IKK complex, perhaps after phagosome-lysosome fusion[16]. Our finding that the actin assembly inhibitor cytochalasin D prolongs AC-induced phospho-p65 is consistent with this idea, as cytochalasin D blocks the internalization of efferocytosis receptor-containing phagosomes[10,11,17,28]. Additional studies are needed to better understand the transient nature of efferocytosis-induced IKK activation and how it differs from pro-inflammatory IKK activation.

One of the downstream resolution pathways resulting from transient activation of IKKβ/NFκB/p38 is PD-L1 induction, which, in this study, links efferocytosis to the pro-resolving process of T_{reg} cell expansion. Interestingly, T_{reg} cells promote efferocytosis[39,50], in part due to T_{reg} cell-stimulated IL-10 production in macrophages[39], suggesting a positive feedback process that complements previously described efferocytosis-resolution feedback pathways[2]. Other pro-resolving processes triggered by the IKKβ pathway include cell-autonomous IL-10 production itself as well as continuing efferocytosis and efferocytosis-induced macrophage proliferation. Each of these processes plays a critical role in tissue resolution in vivo and helps guard against the transition of acute inflammatory conditions to chronic, non-resolving inflammatory diseases[1,2]. An interesting feature of this pathway is the functional integration of its downstream branches, e.g., IL-10 and PD-L1 both contribute to continuing efferocytosis, and PD-L1 also promotes pro-resolving T_{reg} cell expansion. In addition, Myc leads to an increase in both PD-L1 and efferocytosis-induced macrophage proliferation. Previous work has shown that other mechanisms activate some of the above downstream pathways in efferocytosing macrophages, e.g., induction of IL-10 by both oxidative phosphorylation[60] and efferocytosis-induced aryl hydrocarbon receptor activation[11]. In these cases, IL-10 is induced at later timepoints after AC exposure, suggesting the possibility of complementary early-stage and later-stage pro-resolving programming in efferocytosing macrophages. Interestingly, the IKKβ/NFκB/p38 pathway does not mediate efferocytosis-induced TGF-β1[38]. While TGF-β1 can facilitate healing, it can also play a role in pathological fibrosis[61], which IL-10 can mitigate[62]. Thus, the activation of a pro-resolving program that does not include TGF-β1 may be beneficial in specific settings.

Using an inducible knockout model, we have shown that deletion of IKKβ in macrophages specifically during atherosclerosis regression impairs fibrous cap thickening. Previous work has shown that this plaque-stabilizing process, which is highly relevant to humans on intensive LDL-lowering therapy[53–55], is dependent on efferocytosis, pro-resolving pathways, and T_{reg} cells[8–11,50]. In atherosclerosis progression, where the inflammatory state is high and efferocytosis is impaired[63,64], one might predict that the pathway described here is less relevant. However, previous studies found that germline knockout of IKKβ in macrophages exacerbated atherosclerotic plaque progression, whereas germline p65 overexpression in macrophages attenuated plaque progression[65,66]. Efferocytosis and other resolution pathways in the atherosclerotic lesions of the mice from these previous studies were not examined, and thus future work will be needed to understand whether these findings are related to the pathway described here. Related to this issue is whether other actions of IKKβ may contribute to the pro-resolving effects of the pathway relevant to atherosclerosis. Although prolonged expression of inflammatory NFκB-induced cytokines is pro-atherogenic[64], some of these cytokines may activate pro-resolving athero-protective processes when expressed transiently or in specific settings. For example, while IL-1β neutralizing antibodies lower adverse cardiovascular events in humans[67], studies in mice have shown that IL-1β blocking antibodies have a destabilizing effect on advanced atherosclerotic plaques in the setting of atherosclerosis regression[68]. Further studies will be needed to determine if this finding has any link to the pathway described here. Another athero-relevant topic is related to the role of TET2 as a linker between upstream IKKβ and downstream resolution signaling, as loss-of-function (LoF) somatic *TET2* mutations in hematopoietic cells, known as clonal hematopoiesis, are a risk factor for cardiovascular disease in humans[69]. The most widely studied mechanism is inflammasome activation in TET2-LoF macrophages[70,71],

https://doi.org/10.1038/s41467-026-78229-x

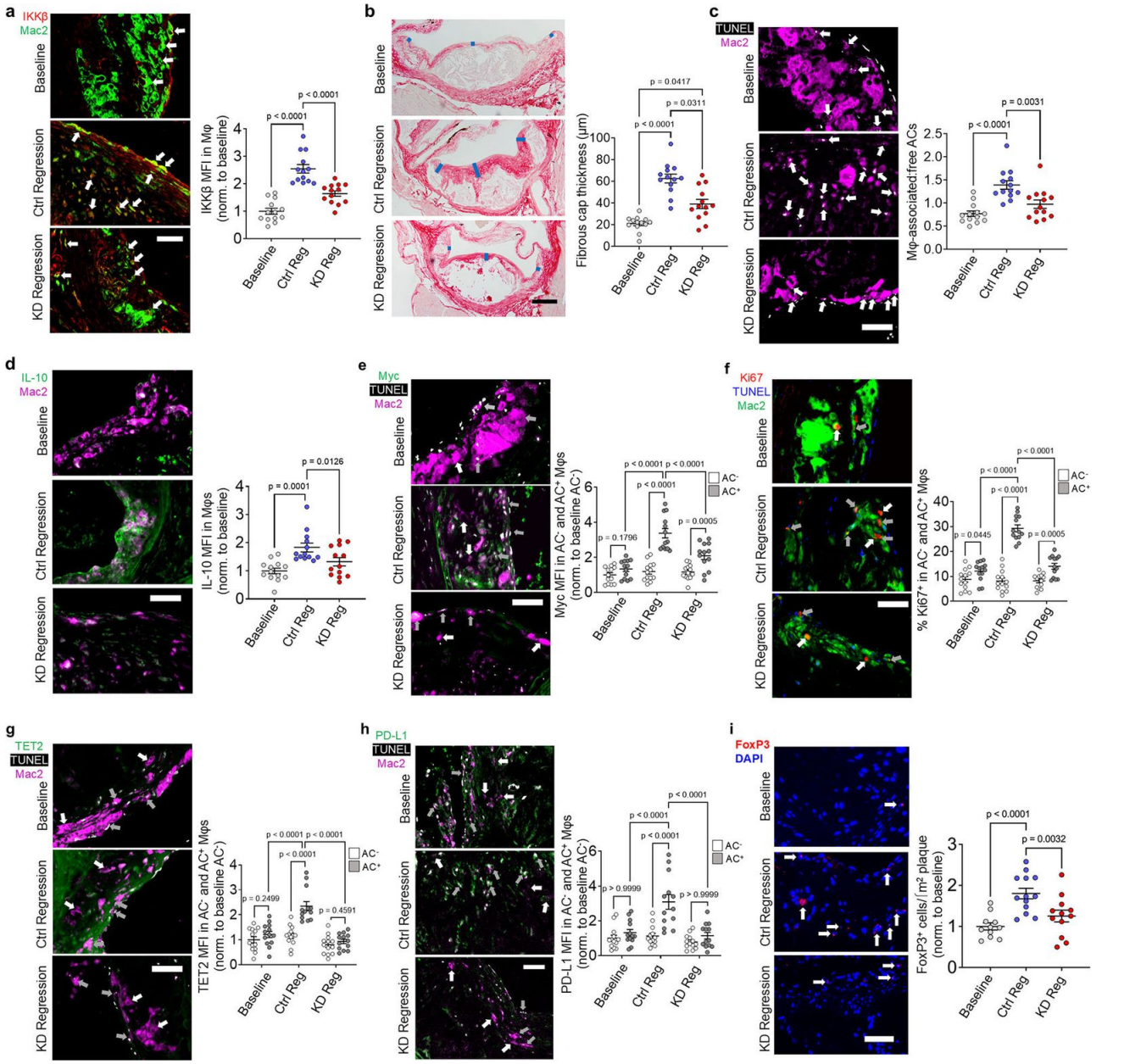


Fig. 9 | The IKKβ pathway contributes to fibrous cap thickening in atherosclerosis regression. a–j *Ldlr*$^{-/-}$ mice transplanted with *Ikbkb*$^{fl/fl}$ (Ctrl) or *Ikbkb*$^{fl/fl}$*;Cx3cr1*$^{CreERT2/+}$ (KD) bone marrow cells were fed the Western diet for 16 weeks. A cohort of Ctrl mice was harvested (baseline), and cohorts of the Ctrl and KD mice were subjected to 7 weeks of LDL lowering to induce atherosclerosis regression. The mice were also given tamoxifen to lower the expression of macrophage IKKβ in the KD cohort ($n = 13$ mice per group). **a** Aortic root plaques were immunostained for IKKβ and Mac2 and quantified for IKKβ MFI in Mac2$^+$ areas. Scale bar, 50 μm. **b** Plaques were stained with picrosirius red to identify the fibrous cap and quantified for fibrous cap thickness, normalized to the baseline value. Scale bar, 200 μm. **c** Plaques were labeled with TUNEL, immunostained for Mac2, and quantified for the ratio of TUNEL$^+$ cells associated with Mac2$^+$ cells to free TUNEL$^+$ cells. Scale bar, 50 μm. **d** Plaques were immunostained for Mac2 and IL-10 and quantified for MFI in Mac2$^+$ areas, normalized to the baseline value. Scale bar, 50 μm. **e** Plaques were labeled with TUNEL, immunostained for Myc, and quantified for Myc MFI in Mac2$^+$ areas that were cTUN$^-$ or cTUN$^+$ (efferocytosing macrophages), normalized to the baseline/AC$^-$ value. **f** As in **e**, except the percent Ki67$^+$ macrophages was quantified. **g** As in **e**, except TET MFI was quantified. **h** As in **e**, except PD-L1 MFI was quantified. In **e**–**h**, white arrows indicate Mac2$^+$ cTUN$^-$ and gray arrows indicate Mac2$^+$ cTUN$^+$ cells; scale bars, 50 μm. **i** Lesions from the three groups of mice were immunostained for FoxP3 and quantified as the number of FoxP3$^+$ cells (arrows) per lesion area, normalized to the baseline value. Scale bar, 50 μm. Bars represent means ± SEM. Statistics were performed using one-way ANOVA for **a**–**d**, **i** and two-way ANOVA for **e**–**h**.

but whether the loss of efferocytosis-induced resolution via the pathway elucidated here contributes to the risk remains to be investigated.

Given the role of impaired efferocytosis and resolution in many types of common diseases[1,2], it is not surprising that both academia and the pharmaceutical industry have devoted increasing effort to devising ways to enhance these processes therapeutically[72–75]. The presence of a common upstream activator of multiple downstream resolution pathways may suggest ways to promote an integrated resolution program efficiently. Moreover, anti-inflammatory drugs, which are used widely for inflammatory and autoimmune diseases and are being tested in atherosclerosis, come at the expense of adverse effects whose mechanisms are not always known[76,77]. Given the findings here, some of the adverse effects may come from impairing efferocytosis-induced resolution, and thus the knowledge gained from

the findings in this study may suggest new strategies to help mitigate these effects.

Methods

Experimental animals

Animal protocols used were approved by Columbia University's Institutional Animal Care and Use Committee and Augusta University Institutional Animal Care and Use Committee and were cared for according to National Institutes of Health (NIH) guidelines for the care and use of laboratory animals. The mice were socially housed in standard cages at 22 °C and with a 12 h light-dark cycle in a barrier facility with ad libitum access to food and water. Male C57BL/6J (JAX, catalogue no. 000664), 8–10 weeks old, were used as bone-marrow transplantation (BMT) recipient mice for the dexamethasone-thymus experiments. Male *Cd274*$^{fl/+}$ and *Cd274*$^{fl/+}$;*LysMCre*$^{+/-}$ bone marrow-donor mice (C57BL/6J background) were generated by crossing *Cd274*$^{fl/fl}$ (JAX, stock no. 036255) with LysMCre (JAX, stock no. 004781). Donor bone marrow from male *Ikbkb*$^{fl/fl}$ or *Ikbkb*$^{fl/fl}$;*Cx3cr1*$^{CreERT2/+}$ mice[78] for BMT were provided by co-authors Dr. Joshua Thaler and Jeremy Frey (University of Washington). Bone marrow preparations from male TET2 WT and KO mice used for generating bone marrow-derived macrophages (BMDM) and for bone marrow transplantation were obtained from Kenneth Walsh and Heather Doviak (University of Virginia)[70,79]. Femurs for isolating BMDMs from male *LysMCre*$^{+/+}$ control and *p65*$^{fl/fl}$;*LysMCre*$^{+/+}$ mice[80] were provided by co-author Jennifer Bradford (Augusta University). Male *Ldlr*$^{-/-}$ mice (JAX, stock no. 002207) were used for atherosclerosis regression studies. All experimental and control animals were housed and bred together. They were then randomly allocated to respective groups. This research complies with all relevant ethical regulations and has been approved by Columbia University's Institutional Animal Care and Use Committee (IACUC).

Euthanasia

Isoflurane was used to completely anesthetize the mice. Deep anesthesia was confirmed by the absence of a pedal withdrawal response following hindlimb toe pinch. The thoracic cavity was then opened using sterile instruments after removal of the chest fur, and blood was be collected from the left ventricle. Subsequent perfusion of the vascular tree with phosphate-buffered saline (PBS) ensured rapid euthanasia. This approach provides a rapid and humane method of sacrifice that minimizes animal distress and complies with the American Veterinary Medical Association (AVMA) Guidelines for the Euthanasia of Animals (Section M1.3, Inhaled Anesthetics). The procedure has been reviewed and approved by the Columbia University IACUC.

Primer sequences, reagents, siRNAs, and antibodies

All primer sequences, reagents, siRNAs, and antibodies are listed in Supplementary Tables 1, 2, 3, and 4, respectively.

Bone marrow transplantation

For the dexamethasone-thymus experiments, 8–10-week-old C57BL/6J male mice were used as the recipients. Recipient mice were irradiated with 10 Gγ with a caesium-137 γ-emitting irradiator (Gamma cell 40, MSD Nordion), and 4–6 h following irradiation, 2.5×10^6 donor bone marrow cells were injected intravenously by tail vein into each recipient mouse. Recipient mice were allowed to recover for 4 weeks and given water containing 10 mg ml^{-1} neomycin for the first 3 weeks. These mice were then used for subsequent experiments.

Dexamethasone-thymus assay

Mice were injected i.p. with 250 µg dexamethasone in PBS, or an equal volume of PBS as a control, and then at 4, 8, or 18 h after injection, the mice were euthanized, and the thymi were harvested and fixed in 10% formalin, embedded in paraffin, and sectioned at a thickness of 5 µm. Sections were then used for H&E staining or immunofluorescence staining for analysis. Regions that were hypocellular or contained fragmented nuclei on H&E-stained sections, which is a measure of tissue necrosis in the thymus, were quantified as the percent of total thymus area. In-situ efferocytosis was quantified as the ratio of Mac2$^+$/CD68$^+$-associated TUNEL$^+$ cells to free TUNEL$^+$ cells.

Mouse bone marrow-derived macrophages

Bone marrow cells were isolated from the femurs of 8–12-week-old male C57BL/6J mice, *LysMCre*$^{+/+}$ mice, *p65*$^{fl/fl}$;*LysMCre*$^{+/+}$ mice, TET2 WT mice, TET2 KO mice, *Cd274*$^{fl/+}$ mice, and *Cd274*$^{fl/+}$;*LysMCre*$^{+/-}$ mice. Bone marrow cells were cultured for 7 days in BMDM differentiation medium, which is composed of DMEM supplemented with 10% (v/v) heat-inactivated fetal bovine serum (HI-FBS), 100 U mL^{-1} penicillin-streptomycin, and 20% (v/v) L-929 cell-conditioned medium. Cells were incubated at 37 °C in a 5% CO_2 incubator.

Human monocyte-derived macrophages

Peripheral blood mononuclear cells were isolated from the buffy coats of anonymous healthy adult donors with informed consent (New York Blood Center) using Histopaque-1077. Isolated cells were rinsed and cultured for 7-14 days in RPMI-1640 medium with L-glutamine supplemented with 10% (v/v) HI-FBS, 100 U mL^{-1} penicillin-streptomycin, and 10 ng/mL GM-CSF. All uses of human material were approved by Columbia University's Institutional Review Board and Health Insurance Portability and Accountability Act guidelines were followed.

Cell lines

L-929 fibroblasts and Jurkat T-lymphocytes were cultured in DMEM supplemented with 10% HI-FBS and 100 U mL^{-1} penicillin-streptomycin. Cells were grown in an incubator at 37 °C with 5% CO_2.

Generation of apoptotic cells and incubation with macrophages

For experiments using apoptotic Jurkat cells, Jurkat cells were resuspended in PBS and irradiated with a 254-nm UV lamp for 15 min to induce apoptosis. To fluorescently label ACs, irradiated ACs were pelleted by centrifugation, resuspended in Diluent C, mixed with Diluent C containing PKH67 (green) or PKH26 (red), and incubated at 37 °C for 5 min. The labeling reaction was quenched by adding an equal volume of HI-FBS. ACs were pelleted, resuspended in PBS, and incubated at 37 °C for 2–3 h. To generate apoptotic HMDMs, differentiated HMDMs were treated with 1 µM staurosporine in RPMI-1640 supplemented with 10% (v/v) HI-FBS and 100 U mL^{-1} penicillin-streptomycin for 48 h. Apoptotic HMDMs were then collected in Cellstripper with gentle scraping. The ACs were then pelleted, resuspended in fresh PBS, and added to macrophages at a 5:1 number ratio of ACs: macrophages and incubated for up to 45 min at 37 °C. The volume ratio of the ACs in PBS to culture medium was 1:10. Unbound ACs were then washed off with PBS and chased for 1, 3, 6, or 24 h in full medium ± the addition of the specified inhibitors.

siRNA transfection

Macrophages were seeded at a confluence of ~60% and transfected with 50 nM scrambled RNA or targeted siRNA (Supplementary Table 3) in Opti-MEM reduced-serum medium using Lipofectamine RNAiMAX. After 18 h, the medium was changed to fresh BMDM-differentiation medium and incubated for an additional 54 h before use.

Cell counting

Macrophages were seeded at 100,000 cells/well in a 12-well plate in full medium and then incubated ± ACs for 45 min and chased for 24 h. The macrophages were then detached with 10 mM EDTA in ice-cold PBS by gentle scraping and counted using a Countess II Automated Cell Counter (Invitrogen; AMQAX1000).

Immunoblotting

Macrophages were lysed in 2x Laemmli sample buffer with 50 mM β-mercaptoethanol, and then the lysates were boiled at 95–100 °C for 5 min. Lysates were loaded onto 4–20% SDS-PAGE gradient gels and run at 120 V for 90 min. Protein was then transferred onto a 0.45-micron nitrocellulose membrane at 250 mA for 100 min or at 90 mA overnight for large proteins. Membranes were blocked for 1 h with 5% skim milk or 5% bovine serum albumin for TET2 immunoblots in Tris-buffered saline with Tween-20 (TBST). Membranes were then incubated overnight at 4 °C with primary antibody diluted in 5% skim milk or 5% bovine serum albumin for TET2. Membranes were washed 3 × 5 min with TBST before incubation with HRP-conjugated secondary antibodies at room temperature for 1–2 h and washed 3 × 5 min with TBST. The following antibodies were used: rabbit anti-phospho p65 S536, rabbit anti-total p65, rabbit anti-phospho p38 T180/Y182, rabbit anti-total p38, rabbit anti-phospho IKKα Ser176/IKKβ Ser177, mouse anti-total IKKβ, rabbit anti-LRP1, rabbit anti-total IKKγ, goat anti-Mer, rabbit anti-phospho STAT3 Y705, mouse anti-total STAT3, rabbit anti-cMyc, rabbit anti-TET2, rabbit anti-IκBα, rabbit anti-Axl, rabbit anti-phospho IRAK4, rabbit anti-total IRAK4, goat anti-MyD88, anti-β-actin HRP-conjugate, anti-α-tubulin HRP-conjugate, anti-rabbit IgG HRP-linked, anti-mouse IgG HRP-linked, anti-rat IgG HRP-linked, and anti-goat IgG HRP-linked.

Co-immunoprecipitation

BMDMs pre-treated with 1 μM UNC5293 or vehicle control for 2 h were incubated ± ACs for 45 min and chased for 0 or 1 h. The cells were then lysed with IP lysis buffer (50 mM Tris pH 7.5, 150 mM NaCl, 0.5 mM EDTA, 1% Triton X-100) supplemented with Halt protease and phosphatase inhibitor cocktail. Lysates were passed through a 25 G needle 5 times and incubated at 4 °C for 15 min before centrifugation at 16,000 × *g* at 4 °C for 10 min. Supernatants were transferred to a clean tube and measured for protein concentration. Before immunoprecipitation, 5 μg isotype control goat IgG antibody or anti-MerTK antibody was crosslinked to protein A magnetic beads. Briefly, 30 μL of protein A magnetic beads were aliquoted to fresh tubes for each IP sample, washed twice with wash buffer (PBS with 0.05% Tween-20, pH 7.4), and resuspended in 200 μL wash buffer. The antibody was then added to the beads, followed by rotating at 4 °C for 1 h, removal of the antibody solution, and washing of the beads twice in wash buffer. The beads were then washed once in crosslink buffer (20 mM sodium phosphate, 150 mM NaCl, pH 7.5). The beads were then resuspended in 250 μL of 5 mM BS3 crosslinker dissolved in crosslink buffer and rotated at room temperature for 1 h. The crosslinking reaction was then quenched with 12.5 μL 1 M Tris-HCl, pH 9.0 and rotated at room temperature for 30 min. The beads were then washed once with 0.2 M glycine-HCl, pH 2.3 and twice with wash buffer. Next, 200 μg of protein from each sample was added to the antibody-crosslinked beads and rotated at 4 °C overnight. The following day, the beads were washed twice with IP lysis buffer, twice with buffer A (50 mM Tris pH 8.0, 250 mM NaCl, 0.1 mM EDTA, 0.1% NP-40, 10% glycerol, 1 mM DTT), and once with buffer B (50 mM Tris pH 8.0, 150 mM NaCl, 0.1 mM EDTA, 0.1% NP-40, 10% glycerol, 1 mM DTT). Protein was eluted from the beads by adding 50 μL 0.1% RapiGest SF surfactant in 200 mM Tris pH 8.0 and then boiling for 10 min. The eluted protein was transferred to a fresh tube, 4x Laemmli buffer was added, and the samples were immunoblotted as above.

Single (primary) and double (continuing) efferocytosis assays

For single efferocytosis assays, PKH26 (red)-labeled ACs were added to macrophages at a 5:1 AC:macrophage ratio for 45 min. Unbound ACs were then removed by rinsing with PBS, and the cells were fixed with 4% paraformaldehyde (PFA) for 10 min at room temperature. For double efferocytosis assays, PKH67 (green)-labeled ACs were added to macrophages for 45 min, unbound ACs were washed off with PBS, macrophages were incubated for 2 h in full medium, PKH26 (red)-labeled ACs were added to the macrophages for 45 min, unbound ACs were washed off with PBS, and the macrophages were then fixed in 4% PFA. For double efferocytosis assays involving cytochalasin D treatment, 5 μM cytochalasin D (CytoD) was added to the culture medium 20 min before the addition of the PKH26-labeled ACs. For both single and double efferocytosis assays, macrophages were subjected to brightfield imaging to identify individual macrophages and fluorescence imaging to identify macrophage uptake of the first and second rounds of ACs using the Leica DMI6000B inverted epifluorescence microscope. Single efferocytosis was quantified as the percentage of total macrophages that had taken up a red AC. Double efferocytosis was quantified as the percentage of macrophages that had taken up a green AC from the first round that had also taken up a red AC from the second round.

Immunofluorescence staining and microscopy

BMDMs seeded on 8-well chamber slides at 80,000 cells per well were pre-treated with 10 μg MerTK neutralizing antibody or goat IgG control antibody for 2 h before the addition of PKH26 (red)-labeled ACs for 45 min and a 6 h chase period. Cells were fixed with 4% PFA for 10 min at room temperature and washed with PBS. To stain cell surface PD-L1, cells were not permeabilized before blocking with 2% bovine serum albumin (BSA) in PBS for 1 h at room temperature. Cells were incubated with anti-PD-L1 primary antibody diluted in blocking solution overnight at 4 °C. The cells were then washed 3 × 5 min with PBS before incubation with goat anti-rat AF488 secondary antibody. After secondary antibody incubation, the cells were washed 3 × 5 min with PBS, incubated for 15 min at room temperature with Hoechst-33342 (1:1000), then mounted with ProLong Gold Antifade Mountant. Cells were imaged using the Zeiss LSM 900 confocal microscope.

For paraffin-embedded tissues, sections were deparaffinized with xylene and rehydrated with 100% ethanol and 70% ethanol before rinsing with PBS. Antigen retrieval was performed using 1x Citrate-Based Antigen Unmasking Solution and pressure cooking for 10 min. For FoxP3 staining of atherosclerotic lesions, antigen retrieval was performed in Tris-based Antigen Unmasking Solution. TUNEL staining was done after antigen retrieval using the In Situ Cell Death Detection Kit according to the manufacturer's instructions. Tissue sections were typically blocked with 2% BSA in PBS, but for FoxP3 of atherosclerotic lesions, we used 1% horse serum in PBS plus 0.3% Triton X-100 for 1 h at room temperature. After blocking, the tissue sections were incubated with primary antibodies diluted in blocking solution overnight at 4 °C. The following primary antibodies were used: rabbit anti-phospho-p65 S536, rabbit anti-phospho-p38 T180/Y182, rat anti-PD-L1, rabbit anti-TET2, rabbit anti-cMyc, mouse anti-IKKβ, rat anti-FoxP3, rabbit anti-CD3, rat anti-Mac2, goat anti-Mac2, rabbit anti-CD68, mouse anti-CD68, rabbit anti-F4/80. Tissue sections were washed 3 × 5 min with PBS before incubation for 2 h at room temperature in the dark with fluorescently labeled secondary antibodies diluted in blocking solution. Tissues were imaged using a Leica epifluorescence microscope (catalogue no. DM16000B). The following secondary antibodies were used: goat anti-mouse AF488, donkey anti-rabbit AF488, donkey anti-goat AF568, goat anti-rabbit AF555, goat anti-rat AF488, goat anti-rat AF647, and donkey anti-rabbit AF647, and donkey anti-rat AF555.

Rac1 activity assay

WT, *Cd274*$^{fl/+}$, or *Cd274*$^{fl/+}$*; LysMCre*$^{+/-}$ BMDMs were plated on 12-well plates and pre-treated ± 0.5 μM IKK16 for 2 h before incubating with unlabeled ACs at a 5:1 ratio for 45 min. After a 2 h chase, the cells were incubated with 6–8 μm phosphatidylserine-coated polystyrene beads for 45 min at a 5:1 ratio of beads:macrophages and then washed with PBS. The macrophages were then lysed, and Rac1 activity was measured with the Rac1 Colorimetric G-LISA Activation Assay Kit according to the manufacturer's instructions.

Reverse transcription-quantitative polymerase chain reaction

RNA was isolated from macrophages using the PureLink RNA Mini kit according to the manufacturer's protocol. The RNA quality and concentration were measured using a NanoDrop spectrophotometer (ThermoFisher). cDNA synthesis was generated from RNA using High-Capacity cDNA Reverse Transcription Kit (ThermoFisher). RT-qPCR was conducted using the QuantStudio 3 Real-Time PCR system (Applied Biosystems) and the Power SYBR Green PCR Master Mix. The primers are listed in Supplementary Table 1. The expression levels of mRNAs of interest were normalized to those of the housekeeping gene *Hprt*.

Atherosclerosis regression

Ldlr$^{-/-}$ mice were transplanted with either *Ikbkb*$^{fl/fl}$ or *Ikbkb*$^{fl/fl}$; *Cx3cr1*$^{CreERT2/+}$ bone marrow and allowed 4 weeks to recover. After recovery, the mice were fed a Western-type diet for 16 weeks. One group of mice was harvested at this point (baseline), while the other two groups were injected i.v. with helper-dependent adenovirus containing the human LDLR gene (HDAd-LDLR) and switched back to chow diet for an additional 7 weeks. To induce *Ikbkb* knockout during regression, mice were injected with 5 mg tamoxifen s.c. twice a week for the duration of the regression period. Before harvesting, each group of mice was fasted overnight, and blood glucose was assayed using the OneTouch Ultra device. After sacrifice, blood was collected by cardiac puncture and used for complete blood count and plasma cholesterol measurements. Blood cell counts were measured by the FORCYTE Hematology Analyzer (Oxford Science), and the plasma cholesterol was measured using a commercially available kit (Supplementary Table 2). Aortic roots were histologically processed for plaque analysis. Parafilm-embedded sections of the aortic roots were stained for H&E and picrosirius red to quantify lesion area, necrotic core area, and fibrous cap thickness. The remaining sections were used for immunofluorescence analysis.

Treatment of macrophages with Gas6

Conditioned medium containing g-carboxylated Gas6 was harvested from human Gas6-expressing HEK 293-6E cells incubated with vitamin K (2 mg/ml), as described previously[81].

IL-10 ELISA

BMDMs were plated at a density of 500,000 cells per well in a 12 well cell-culture plate and pretreated either with vehicle control or 500 nM IKK16 for 2 h. The macrophages were then incubated ± ACs at a 5:1 ratio and, after 45 min, the wells were washed and fresh DMEM media was added. After 4 h of further incubation (chase), the conditioned media were collected. The media was first passed through Pierce Protein Concentrators 3 K Molecular Weight Cut Off PES columns and then subjected to an ELISA assay using the Duo Set Mouse IL-10 ELISA kit as per manufacturer's protocol.

pHrodo staining

BMDMs were plated at a density of 80,000 cells per well in Millicell EZ Slide chamber slides. The cells were pretreated with vehicle control or 500 nM IKK16 for 2 h. During this period, Jurkat cells were induced to undergo apoptosis (above) and then resuspended in PBS and incubated with 5 µl pHrodo Red for 30 min at 37 °C. The labelled Jurkat cells were then rinsed twice with DMEM supplemented with 10% FBS and added to BMDMs at a ratio of 5:1 for 45 min. After rinsing, the macrophages were viewed using a Leica DMI6000B inverted epi-fluorescence microscope and quantified for intracellular pHrodo fluorescence.

Quantification and statistical analysis

GraphPad Prism software (v.9.4.0 and v.9.4.1) was used for all statistical analyses. Data were tested for normality using the Shapiro–Wilk test. Data that passed the normality test were analysed using the two-tailed Student's *t*-test for comparison of two groups or one- or two-way analysis of variance (ANOVA) with Fisher's Least Significant Difference (LSD) post-hoc analysis for comparison of more than two groups. Data that were not normally distributed were analysed using the Mann-Whitney test for 2 groups or the Kruskal-Wallis test followed by uncorrected Dunn's post-hoc analysis for >2 groups. Data are shown as mean values ± s.e.m. for normally distributed data and median values ± interquartile range (IQR) for non-normally distributed data. Differences were considered statistically significant at $P < 0.05$. As indicated in the figure legends, some values are reported relative to the first control group in each experiment. No data were excluded. Data collection and analysis were not performed blind to the conditions of the experiments. *N*-number for the in vitro experiments, which is 3 or 4 depending on the experiment, refers to the number of separate wells of macrophages and was based on many previous studies using the reported assays. The number of mice used for the dexamethasone-thymus assay and mouse atherosclerosis regression studies was determined based on power calculations, with an expected 15–25% coefficient of variation and an 80% chance of detecting a 33% difference in key parameters, including in-situ efferocytosis, necrotic area, and fibrous cap thickness for atherosclerosis regression. For the cell culture studies, no statistical methods were used to predetermine sample sizes, but our sample sizes are similar to those reported in previous publications[9,10].

Reporting summary

Further information on research design is available in the Nature Portfolio Reporting Summary linked to this article.

Data availability

All data are included in the Supplementary Information or available from the authors, as are unique reagents used in this Article. The raw numbers for charts and graphs are available in the Source Data file (provided with the paper) whenever possible. Uncropped gels are provided in the Source Data file. Source data are provided with this paper.

References

1. Morioka, S., Maueroder, C. & Ravichandran, K. S. Living on the edge: efferocytosis at the interface of homeostasis and pathology. *Immunity* **50**, 1149–1162 (2019).
2. Doran, A. C., Yurdagul, A. Jr. & Tabas, I. Efferocytosis in health and disease. *Nat. Rev. Immunol.* **20**, 254–267 (2020).
3. Arandjelovic, S. & Ravichandran, K. S. Phagocytosis of apoptotic cells in homeostasis. *Nat. Immunol.* **16**, 907–917 (2015).
4. Boada-Romero, E., Martinez, J., Heckmann, B. L. & Green, D. R. The clearance of dead cells by efferocytosis. *Nat. Rev. Mol. Cell Biol.* **21**, 398–414 (2020).
5. Dalli, J. & Serhan, C. N. Pro-resolving mediators in regulating and conferring macrophage function. *Front. Immunol.* **8**, 1400 (2017).
6. Park, D. et al. Continued clearance of apoptotic cells critically depends on the phagocyte Ucp2 protein. *Nature* **477**, 220–224 (2011).
7. Wang, Y. et al. Mitochondrial fission promotes the continued clearance of apoptotic cells by macrophages. *Cell* **171**, 331–345 e322 (2017).
8. Yurdagul, A. Jr. et al. Macrophage metabolism of apoptotic cell-derived arginine promotes continual efferocytosis and resolution of injury. *Cell Metab.* **31**, 518–533 e510 (2020).
9. Gerlach, B. D. et al. Efferocytosis induces macrophage proliferation to help resolve tissue injury. *Cell Metab.* **33**, 2445–2463 e2448 (2021).

10. Ampomah, P. B. et al. Macrophages use apoptotic cell-derived methionine and DNMT3A during efferocytosis to promote tissue resolution. *Nat. Metab.* **4**, 444–457 (2022).
11. Sukka, S. R. et al. Efferocytosis drives a tryptophan metabolism pathway in macrophages to promote tissue resolution. *Nat. Metab.* **6**, 1736–1755 (2024).
12. Schilperoort, M., Ngai, D., Katerelos, M., Power, D. A. & Tabas, I. PFKFB2-mediated glycolysis promotes lactate-driven continual efferocytosis by macrophages. *Nat. Metab.* **5**, 431–444 (2023).
13. Ngai, D., Schilperoort, M. & Tabas, I. Efferocytosis-induced lactate enables the proliferation of pro-resolving macrophages to mediate tissue repair. *Nat. Metab.* **5**, 2206–2219 (2023).
14. Zhang, S. et al. Efferocytosis fuels requirements of fatty acid oxidation and the electron transport chain to polarize macrophages for tissue repair. *Cell Metab.* **29**, 443–456 e445 (2018).
15. Morioka, S. et al. Efferocytosis induces a novel SLC program to promote glucose uptake and lactate release. *Nature* **563**, 714–718 (2018).
16. Elliott, M. R. & Ravichandran, K. S. The dynamics of apoptotic cell clearance. *Dev. Cell* **38**, 147–160 (2016).
17. Yurdagul, A. et al. Macrophage metabolism of apoptotic cell-derived arginine promotes continual efferocytosis and resolution of injury. *Cell Metab.* **31**, 518–533.e510 (2020).
18. Karin, M. & Delhase, M. The I kappa B kinase (IKK) and NF-kappa B: key elements of proinflammatory signalling. *Semin. Immunol.* **12**, 85–98 (2000).
19. Waelchli, R. et al. Design and preparation of 2-benzamido-pyrimidines as inhibitors of IKK. *Bioorg. Med. Chem. Lett.* **16**, 108–112 (2006).
20. Maubach, G., Schmädicke, A. C. & Naumann, M. NEMO links nuclear factor-κB to human diseases. *Trends Mol. Med.* **23**, 1138–1155 (2017).
21. Lin, J. et al. MerTK-mediated efferocytosis promotes immune tolerance and tumor progression in osteosarcoma through enhancing M2 polarization and PD-L1 expression. *Oncoimmunology* **11**, 2024941 (2022).
22. Gould, G. W., Cuenda, A., Thomson, F. J. & Cohen, P. The activation of distinct mitogen-activated protein kinase cascades is required for the stimulation of 2-deoxyglucose uptake by interleukin-1 and insulin-like growth factor-1 in KB cells. *Biochem. J.* **311**, 735–738 (1995).
23. Yurdagul, A. Jr. et al. ODC (ornithine decarboxylase)-dependent putrescine synthesis maintains MerTK (MER tyrosine-protein kinase) expression to drive resolution. *Arterioscler Thromb. Vasc. Biol.* **41**, e144–e159 (2021).
24. Zhou, L. & Matsushima, G. K. Tyro3, Axl, and Mertk receptor-mediated efferocytosis and immune regulation in the tumor environment. *Int. Rev. Cell Mol. Biol.* **361**, 165–210 (2021).
25. Lemke, G. & Rothlin, C. V. Immunobiology of the TAM receptors. *Nat. Rev. Immunol.* **8**, 327–336 (2008).
26. Zheng, H. et al. UNC5293, a potent, orally available, and highly MERTK-selective inhibitor. *Eur. J. Med. Chem.* **220**, 113534 (2021).
27. Chen, J., Carey, K. & Godowski, P. J. Identification of Gas6 as a ligand for Mer, a neural cell adhesion molecule related receptor tyrosine kinase implicated in cellular transformation. *Oncogene* **14**, 2033–2039 (1997).
28. Schilperoort, M., Ngai, D., Katerelos, M., Power, D. A. & Tabas, I. PFKFB2-mediated glycolysis promotes lactate-driven continual efferocytosis by macrophages. *Nat. Metab* **5**, 431–444 (2023).
29. Balka, K. R. & De Nardo, D. Understanding early TLR signaling through the Myddosome. *J. Leukoc. Biol.* **105**, 339–351 (2019).
30. Xie, L. et al. Targeting of MyD88 homodimerization by novel synthetic inhibitor TJ-M2010-5 in preventing colitis-associated colorectal cancer. *J. Natl. Cancer Inst.* **108**, djv364 (2016).
31. Bennett, J. et al. Paralog-specific signaling by IRAK1/4 maintains MyD88-independent functions in MDS/AML. *Blood* **142**, 989–1007 (2023).
32. Saraiva, M. et al. Identification of a macrophage-specific chromatin signature in the IL-10 locus. *J. Immunol.* **175**, 1041–1046 (2005).
33. Foey, A. D. et al. Regulation of monocyte IL-10 synthesis by endogenous IL-1 and TNF-alpha: role of the p38 and p42/44 mitogen-activated protein kinases. *J. Immunol.* **160**, 920–928 (1998).
34. Hedrich, C. M. et al. Stat3 promotes IL-10 expression in lupus T cells through trans-activation and chromatin remodeling. *Proc. Natl. Acad. Sci. USA* **111**, 13457–13462 (2014).
35. Ananieva, O. et al. The kinases MSK1 and MSK2 act as negative regulators of Toll-like receptor signaling. *Nat. Immunol.* **9**, 1028–1036 (2008).
36. Kim, C. et al. The kinase p38 alpha serves cell type-specific inflammatory functions in skin injury and coordinates pro- and anti-inflammatory gene expression. *Nat. Immunol.* **9**, 1019–1027 (2008).
37. Schust, J., Sperl, B., Hollis, A., Mayer, T. U. & Berg, T. Stattic: a small-molecule inhibitor of STAT3 activation and dimerization. *Chem. Biol.* **13**, 1235–1242 (2006).
38. Fadok, V. A. et al. Macrophages that have ingested apoptotic cells in vitro inhibit proinflammatory cytokine production through autocrine/paracrine mechanisms involving TGF-beta, PGE2, and PAF. *J. Clin. Investig.* **101**, 890–898 (1998).
39. Proto, J. D. et al. Regulatory T cells promote macrophage efferocytosis during inflammation resolution. *Immunity* **49**, 666–677.e666 (2018).
40. Jeelani, I. et al. HIF-2α drives hepatic Kupffer cell death and proinflammatory recruited macrophage activation in nonalcoholic steatohepatitis. *Sci. Transl. Med.* **16**, eadi0284 (2024).
41. Zhang, C. R. et al. Cancer cell phagocytosis induces an anti-inflammatory gene regulatory program in macrophages. Preprint at *bioRxiv* https://doi.org/10.1101/2025.08.18.670953 (2025).
42. Tu, M. et al. 4-octyl itaconate promotes diabetic wound healing by enhancing pro-resolving macrophages via the efferocytosis-MCT1-lactate-GPR132 pathway and macrophage-independent synergistic effects. *Diabetes Metab J.* **50**, 707–723 (2025).
43. Liu, Y. et al. PARP inhibition synergizes with CD47 blockade to promote phagocytosis by tumor-associated macrophages in homologous recombination-proficient tumors. *Life Sci.* **326**, 121790 (2023).
44. Zhang, D. et al. TIMD4(hi)MHCII(hi) macrophages preserve heart function through Retnla. *JACC Basic Transl. Sci.* **10**, 65–84 (2025).
45. Zeng, L. et al. IRG1/itaconate enhances efferocytosis by activating Nrf2-TIM4 signaling pathway to alleviate con A induced autoimmune liver injury. *Cell Commun. Signal.* **23**, 63 (2025).
46. Yin, Z. et al. EDIL3/Del-1 prevents aortic dissection through enhancing internalization and degradation of apoptotic vascular smooth muscle cells. *Autophagy* **20**, 2405–2425 (2024).
47. Lyss, G., Knorre, A., Schmidt, T. J., Pahl, H. L. & Merfort, I. The anti-inflammatory sesquiterpene lactone helenalin inhibits the transcription factor NF-kappaB by directly targeting p65. *J. Biol. Chem.* **273**, 33508–33516 (1998).
48. Hartley, G. P., Chow, L., Ammons, D. T., Wheat, W. H. & Dow, S. W. Programmed cell death ligand 1 (PD-L1) signaling regulates macrophage proliferation and activation. *Cancer Immunol. Res.* **6**, 1260–1273 (2018).
49. Francisco, L. M. et al. PD-L1 regulates the development, maintenance, and function of induced regulatory T cells. *J. Exp. Med.* **206**, 3015–3029 (2009).
50. Sharma, M. et al. Regulatory T cells license macrophage pro-resolving functions during atherosclerosis regression. *Circ. Res.* **127**, 335–353 (2020).
51. Wu, Z., Cheng, S., Wang, S., Li, W. & Liu, J. C-MYC ameliorates ventricular remodeling of myocardial infarction rats via binding to

the promoter of microRNA-29a-3p to facilitate TET2 expression. *Int. J. Cardiol.* **357**, 105–112 (2022).
52. Tseng, Y. H. et al. Promoter methylation and increased expression of PD-L1 in patients with active tuberculosis. *Micro. Cell* **11**, 278 (2024).
53. Fisher, E. A. Regression of atherosclerosis: the journey from the liver to the plaque and back. *Arterioscler Thromb. Vasc. Biol.* **36**, 226–235 (2016).
54. Puri, R. et al. Factors underlying regression of coronary atheroma with potent statin therapy. *Eur. Heart J.* **34**, 1818–1825 (2013).
55. Sun, M. & Yu, Z. Unraveling the temporal sequence of coronary atherosclerosis modification with lipid-lowering therapies through intravascular imaging: a narrative review. *Front. Cardiovasc. Med.* **13**, 1737177 (2026).
56. Fredman, G. et al. An imbalance between specialized pro-resolving lipid mediators and pro-inflammatory leukotrienes promotes instability of atherosclerotic plaques. *Nat. Commun.* **7**, 12859 (2016).
57. Feig, J. E. et al. Regression of atherosclerosis is characterized by broad changes in the plaque macrophage transcriptome. *PLoS ONE* **7**, e39790 (2012).
58. Sen, P. et al. Apoptotic cells induce Mer tyrosine kinase-dependent blockade of NF-kappaB activation in dendritic cells. *Blood* **109**, 653–660 (2007).
59. Tibrewal, N. et al. Autophosphorylation docking site Tyr-867 in Mer receptor tyrosine kinase allows for dissociation of multiple signaling pathways for phagocytosis of apoptotic cells and down-modulation of lipopolysaccharide-inducible NF-kappaB transcriptional activation. *J. Biol. Chem.* **283**, 3618–3627 (2008).
60. Zhang, S. et al. Efferocytosis fuels requirements of fatty acid oxidation and the electron transport chain to polarize macrophages for tissue repair. *Cell Metab.* **29**, 443–456.e445 (2019).
61. Dewidar, B., Meyer, C., Dooley, S. & Meindl-Beinker, A. N. TGF-β in hepatic stellate cell activation and liver fibrogenesis. *Cells* **8**, 1419 (2019).
62. Wang, S. C., Ohata, M., Schrum, L., Rippe, R. A. & Tsukamoto, H. Expression of interleukin-10 by in vitro and in vivo activated hepatic stellate cells. *J. Biol. Chem.* **273**, 302–308 (1998).
63. Tabas, I. Consequences and therapeutic implications of macrophage apoptosis in atherosclerosis: the importance of lesion stage and phagocytic efficiency. *Arterioscler Thromb. Vasc. Biol.* **25**, 2255–2264 (2005).
64. Libby, P. Inflammation during the life cycle of the atherosclerotic plaque. *Cardiovasc Res.* **117**, 2525–2536 (2021).
65. Kanters, E. et al. Inhibition of NF-kappaB activation in macrophages increases atherosclerosis in LDL receptor-deficient mice. *J. Clin. Investig.* **112**, 1176–1185 (2003).
66. Ye, X., Jiang, X., Guo, W., Clark, K. & Gao, Z. Overexpression of NF-κB p65 in macrophages ameliorates atherosclerosis in apoE-knockout mice. *Am. J. Physiol. Endocrinol. Metab.* **305**, E1375–E1383 (2013).
67. Ridker, P. M. et al. Antiinflammatory therapy with canakinumab for atherosclerotic disease. *N. Engl. J. Med.* **377**, 1119–1131 (2017).
68. Karnewar, S. et al. IL-1β inhibition partially negates the beneficial effects of diet-induced atherosclerosis regression in mice. *Arterioscler Thromb. Vasc. Biol.* **44**, 1379–1392 (2024).
69. Jaiswal, S. et al. Clonal hematopoiesis and risk of atherosclerotic cardiovascular disease. *N. Engl. J. Med.* **377**, 111–121 (2017).
70. Fuster, J. J. et al. Clonal hematopoiesis associated with TET2 deficiency accelerates atherosclerosis development in mice. *Science* **355**, 842–847 (2017).
71. Yalcinkaya, M. et al. BRCC3-mediated NLRP3 deubiquitylation promotes inflammasome activation and atherosclerosis in Tet2 clonal hematopoiesis. *Circulation* **148**, 1764–1777 (2023).
72. Mehrotra, P. & Ravichandran, K. S. Drugging the efferocytosis process: concepts and opportunities. *Nat. Rev. Drug Discov.* **21**, 601–620 (2022).
73. Serhan, C. N. Treating inflammation and infection in the 21st century: new hints from decoding resolution mediators and mechanisms. *FASEB J.* **31**, 1273–1288 (2017).
74. Fredman, G. & Tabas, I. Boosting inflammation resolution in atherosclerosis: the next frontier for therapy. *Am. J. Pathol.* **187**, 1211–1221 (2017).
75. Saas, P., Vetter, M., Maraux, M., Bonnefoy, F. & Perruche, S. Resolution therapy: harnessing efferocytic macrophages to trigger the resolution of inflammation. *Front. Immunol.* **13**, 1021413 (2022).
76. Joseph, D., Tintinger, G. R., Ker, J. A. & Pannell, N. Adverse effects of biologic anti-inflammatory agents on the respiratory system: a review. *Afr. J. Thorac Crit. Care Med.* **27**, 10 (2021).
77. Roubille, C., Martel-Pelletier, J., Davy, J. M., Haraoui, B. & Pelletier, J. P. Cardiovascular adverse effects of anti-inflammatory drugs. *Antiinflamm Antiallergy Agents Med. Chem.* **12**, 55–67 (2013).
78. Arkan, M. C. et al. IKK-beta links inflammation to obesity-induced insulin resistance. *Nat. Med.* **11**, 191–198 (2005).
79. Ko, M. et al. Ten-Eleven-Translocation 2 (TET2) negatively regulates homeostasis and differentiation of hematopoietic stem cells in mice. *Proc. Natl. Acad. Sci. USA* **108**, 14566–14571 (2011).
80. Korkaya, A. K. et al. Production of a p65(fl/fl)/LysMCre mouse model with dysfunctional NF-κB signaling in bone marrow-derived macrophages. *Innate Immun.* **29**, 171–185 (2023).
81. Tsou, W. I. et al. Receptor tyrosine kinases, TYRO3, AXL, and MER, demonstrate distinct patterns and complex regulation of ligand-induced activation. *J. Biol. Chem.* **289**, 25750–25763 (2014).

Acknowledgements

We thank Dr. Xiaobo Wang (Columbia University) for assisting with the BMT and regression experiments; Dr. Raymond Birge (Rutgers New Jersey Medical School) for supplying recombinant gamma-carboxylated Gas6 conditioned media; Dr. Caisheng Lu (Columbia University) for assistance with flow cytometry; and Dr. Adam Mor (Columbia University) for assistance with confocal microscopy using the Zeiss LSM 900 microscope.

Author contributions

This study was conceptualized by D.N., S.C., and I.T. D.N. and S.C. performed experiments, data collection, and data analysis for the majority of the study. D.N., S.C., and B.H. performed staining of tissues and image analysis. G.K. assisted with tissue harvesting for all in vivo studies. S.R.S. performed and analyzed the data from the Rac1 assay using control and PD-L1 Het BMDMs and also performed $CD3^+$ staining of mouse atherosclerotic lesions. M.Y. and A.T. contributed intellectually to this study and provided feedback on the experiments related to TET2 and atherosclerosis. J.M.F. and J.P.T. collected and provided bone marrow from $Ikbkb^{fl/fl}$ and $Ikbkb^{fl/fl}$;$Cx3cr1^{CreERT2/+}$ mice for the Dex-thymus and atherosclerosis regression experiments. H.D. and K.W. provided TET2 WT and TET2 KO bone marrow to generate BMDMs and for BMT in a Dex-thymus experiment. J.W.B. provided $LysMCre^{+/+}$ and $p65^{fl/fl}$; $LysMCre^{+/+}$ bone marrow to generate BMDMs. J.M.F., J.P.T., H.D., and K.W. provided advice on the use of the materials they sent to us, and B.D., H.W., and L.M. provided advice on the analysis of atherosclerotic lesions.

Funding

This work was supported by NIH/NHLBI grant nos. R35-HL145228 and P01-HL17274I (to A.R.T. and I.T.) and American Heart Association Postdoctoral Fellowship Award (to D.N.). Funding for J.W.B. was provided by the Augusta University Foundation. Immunofluorescent imaging experiments with tissue staining were conducted in the Columbia Center for Translational Immunology Core Facility, funded by NIH grant nos. P30CA013696, S10RR027050 and S10OD020056. Samples for

histological analysis were prepared in the Molecular Pathology Shared Resource of the Herbert Irving Comprehensive Cancer Center at Columbia University, supported by NIH grant no. P30CA013696.

Competing interests
The authors declare no competing interests.

Additional information
Supplementary information The online version contains supplementary material available at https://doi.org/10.1038/s41467-026-78229-x.

Correspondence and requests for materials should be addressed to Ira Tabas.

Peer review information *NatureCommunications* thanks Stamatia Papoutsopoulou who co-reviewed with Evangelos Tsioupros; Claudia Monaco, Shao-Cong Sun and the other anonymous, reviewer for their contribution to the peer review of this work. A peer review file is available.

Reprints and permissions information is available at http://www.nature.com/reprints

Publisher's note Springer Nature remains neutral with regard to jurisdictional claims in published maps and institutional affiliations.

Open Access This article is licensed under a Creative Commons Attribution-NonCommercial-NoDerivatives 4.0 International License, which permits any non-commercial use, sharing, distribution and reproduction in any medium or format, as long as you give appropriate credit to the original author(s) and the source, provide a link to the Creative Commons licence, and indicate if you modified the licensed material. You do not have permission under this licence to share adapted material derived from this article or parts of it. The images or other third party material in this article are included in the article's Creative Commons licence, unless indicated otherwise in a credit line to the material. If material is not included in the article's Creative Commons licence and your intended use is not permitted by statutory regulation or exceeds the permitted use, you will need to obtain permission directly from the copyright holder. To view a copy of this licence, visit http://creativecommons.org/licenses/by-nc-nd/4.0/.

© The Author(s) 2026

This Article in Press is shared early to give you faster access to new research. It is citable and carries a permanent DOI. The final edited version will replace it automatically.